Progress in Materials Science 83 (2016) 236–269

Contents lists available at ScienceDirect

Progress in Materials Science

journal homepage: www.elsevier.com/locate/pmatsci

Advanced polymeric dielectrics for high energy density applications

Tran Doan Huan [a,b], Steve Boggs [b], Gilbert Teyssedre [c], Christian Laurent [c], Miko Cakmak [d], Sanat Kumar [e], Rampi Ramprasad [a,b,*]

[a] Department of Materials Science and Engineering, University of Connecticut, Storrs, CT 06269, USA
[b] Institute of Materials Science, University of Connecticut, Storrs, CT 06269, USA
[c] Université de Toulouse, UPS, INPT, LAPLACE (Laboratoire Plasma et Conversion d'Energie), 118 route de Narbonne, F-31062 Toulouse cedex 9, France
[d] Department of Polymer Engineering, University of Akron, 250 South Forge St, Akron, USA
[e] Department of Chemical Engineering, Columbia University, New York, NY 10027, USA

ARTICLE INFO

Article history:
Received 30 October 2015
Received in revised form 22 April 2016
Accepted 1 May 2016
Available online 4 May 2016

Keywords:
Polymer
Dielectric
Energy storage

ABSTRACT

This article provides an overview of the present state-of-the-art pertaining to polymer capacitor dielectrics appropriate for high electrostatic energy density applications. The challenges and opportunities surrounding capacitor materials development/discovery in a practical context are reviewed. It is pointed out that several hierarchical considerations ranging from dielectric, electronic, morphological, processing, reliability and electrical characteristics need to be confronted and addressed adequately before one can progress from "standard" materials (such as biaxially oriented polypropylene) toward next generation materials. Nevertheless, it is argued that the prospects for systematic approaches toward polymer dielectrics discovery appear to be strong, especially given recent successes and evidence that a cooperative computation-synthesis-processing-characterization paradigm can bear fruit. It is hoped that this article will be particularly useful for a new researcher entering the field as it presents a snapshot of various critical aspects of this emerging field in one comprehensive narrative.

Contents

* Corresponding author at: Department of Materials Science and Engineering, University of Connecticut, Storrs, CT 06269, USA.
E-mail address: rampi.ramprasad@uconn.edu (R. Ramprasad).

http://dx.doi.org/10.1016/j.pmatsci.2016.05.001
0079-6425/

1. Introduction

1.1. Early history

The most important concepts of electrostatic energy storage came very early in the history of electrostatic capacitors and include Benjamin Franklin's realization that the water of the Leyden Jar (1746) was not necessary to energy storage. This resulted in Franklin's flat metallic foil–glass capacitors of the early 1750s. Electrolytic capacitor technology started with Pollak who, in 1887, submitted a patent on an electrolytic capacitor that included a complete and thoroughly modern description of its function [1]. The first patent on a "self-clearing" capacitor dielectric (i.e., recovery from breakdown of the dielectric) dates back to 1900 by Mansbridge [2]. Thus by the turn of the 20th century, many of the key technologies used in present electrostatic energy storage were known; however, the storage media, dominated by wax paper–metal foil for filter applications (1876) [3] and silver–mica (1909) for radio frequency (RF) coupling, were of very low energy density. Even early electrolytic capacitors were of low energy density, as they consisted of a bulk liquid electrolyte between metal electrodes. The modern wound electrolytic capacitor with an electrolyte-impregnated separator was patented in 1927 [4].

The first application of polymers in capacitor technology was lacquer applied to paper in order to improve insulation resistance and inhibit moisture-related electrolytic corrosion of metalized paper capacitors (Bosch, WWII). The first polymer film capacitor was based on lacquer separated from paper employed as a 2.5 μm, polymeric dielectric by the Bell System around 1954. Polymer technology evolved rapidly after about 1950, and by 1959, capacitors were being manufactured with polyethylene (PE), polystyrene (PS), polytetrafluoroethylene (PTFE), polyethylene terephthalate (PET), and polycarbonate (PC) films, and later, biaxially oriented polypropylene (BOPP), which presently dominates high energy density applications. Fig. 1 presents a timeline of the early capacitor development history. The early history of capacitors after the mass market for consumer electronics (radio) constitutes a search for improved technologies with greater energy density and reduced cost. This search is still on with increased operating temperature added to the list of important criteria. Presently, the search for improved technology is motivated largely by consumer (e.g., hybrid/electric vehicles and consumer electronics) and

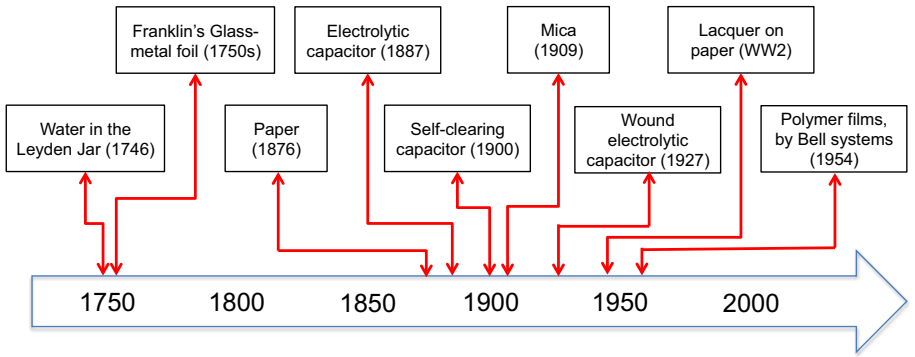

Fig. 1. Early history of capacitor development.

industrial applications (e.g., variable speed drives and other forms of power conversion), although military applications of such technology motivates a great deal of military funding.

1.2. General background

A capacitor or condenser is a two-terminal device that stores electric charge in proportion to the electric potential between its terminals, i.e., $Q = CV$ where Q is the charge, C is the capacitance and V is the electric potential. Capacitors store electrostatic energy, given $\frac{1}{2}CV^2$ within a dielectric between the two terminals. The dielectric can be a ceramic, polymer film, electric double layer at a liquid-conductor interface, etc. In a parallel-plate capacitor in which the dielectric is housed between the two terminal electrodes spaced by a distance d and with cross-sectional area A, $C = \varepsilon A/d$, where ε is the absolute dielectric constant. The electrostatic energy density within the dielectric if it is *linear*, i.e., if ε is independent of the electric field $E = V/d$, is $\frac{1}{2}\varepsilon E^2$.

Polymer dielectrics found in metallized film capacitors form the focal point of this review. The choice of polymers (over ceramics) in many capacitive energy storage applications is motivated by the need for "graceful failure" of the dielectric at high fields. Metallized polymers offer the only scalable self-clearing capacitor technology that meets this need. Fig. 2 shows a schematic of such a metallized capacitor winding (left) and a bank of capacitor windings found in a typical hybrid electric vehicle.

The "push" for improved capacitor dielectrics centers on three high-level (component-level) requirements:

- Improved maximum operating temperature to facilitate improved thermal management in power electronics, heat sinking to engine cooling loops in automotive applications, improved performance in military systems, etc.
- Increased operating electrostatic energy density, which means increased dielectric constant with low loss and without reducing operating field. This is important for pulsed power applications, power electronics, etc.
- Increased thermal conductivity, especially in the plane of the film transverse to the direction of extrusion, i.e., transverse to the machine direction. In many applications, most heat flows along the film to the end connections, and thermal conductivity in the axial direction of the capacitor is very important.

Fig. 2. (Left) Single-section winding showing more heavily metalized edges region, lightly metalized active region, and an unmetalized margin. The two layers are offset so that the heavily metalized region at the top protrudes beyond the layer below. (Right) A bank of metallized capacitor windings found in a typical hybrid electric vehicle.

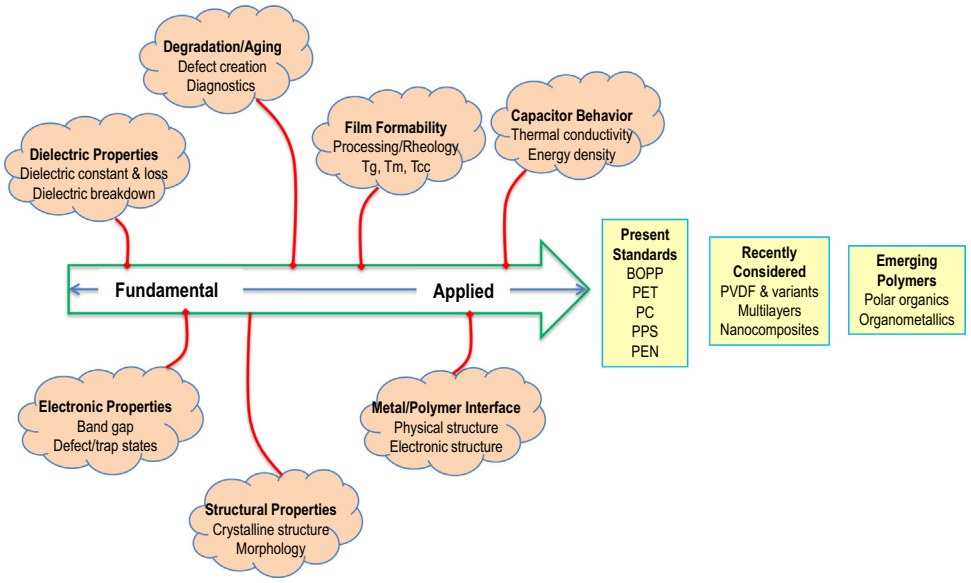

Fig. 3. Spectrum of fundamental-to-applied attributes that is used to evaluate a successful capacitor material. On the right is a selected listing of the current standard materials, recently studied materials, and emerging polymer subclasses.

Needless to say, these *component-level* requirements translate to specific *materials-level* attributes, including constraints on the dielectric constant, dielectric breakdown field, dielectric loss, defect content (and their effects), electronic structure, glass transition and melting temperatures, polymer morphology and rheology, intrinsic thermal conductivity, etc. Moreover, areas in need of improvement are not independent. Properties such as thermal conductivity need to improve in parallel with increased dielectric constant and certainly cannot decrease in exchange for greater dielectric constant for a film dielectric to be viable in power applications. While a general solution that meets the needs of all high energy density applications does not (and may not) exist, any improvement over the present technology for specific applications must be consistent with majority of the materials-specific needs, i.e., new materials must be evaluated in the context of likely applications. Fig. 3 shows the material requirements for polymeric capacitor dielectrics grouped within classes of properties/behaviors arranged hierarchically, going from fundamental to more practical aspects in a spectrum of evaluation steps that, hopefully, will lead to useful materials. At the most basic level, potential candidates are required to have favorable dielectric and electronic properties, which are the attributes that may be determined/estimated by first-principles computations. More empirical (computational and/or experimental) methods are needed to assess material properties at higher levels of complexity, e.g., structural morphology, metal/polymer interfaces, and degradation/aging processes. Film formability and capacitor performance, the highest-level properties in the hierarchy, are largely determined by appropriate experimental methods as theoretical/computational approaches for these aspects remain inadequate. For a prototype capacitor material to become widely useful, it must "pass" these successive evaluation steps.

1.3. Present state-of-the-art

The market for high energy density dielectrics, such as polymer films, is rarely sufficient to motivate manufacture solely for that purpose, and nearly all commercial dielectrics are based on consumer or commercial technology, although special material grades are often manufactured for dielectric applications. The manufacture of dielectric films requires advanced manufacturing technology to obtain uniform thickness over a wide web of film processed at high speed with available film thicknesses from sub-micron to tens of microns depending on the polymer. Table 1 summarizes the properties of some

Table 1
Properties of common capacitor dielectrics, including the glass transition temperature (T_g), melting temperature of the polymer crystals (T_m), fraction of crystallites in the morphology, relative dielectric permittivity (ϵ), dielectric loss, and the dielectric breakdown field (E_{bd}).

Polymer	T_g (°C)	T_m (°C)	Crystallinity	ϵ	Loss (@25 °C) (%)	E_{bd} (MV/m)
BOPP	<25	160	>0.6	2.25	0.02	720
PET	75–80	255	~0.5	3.2	0.35	570
PC	145–150	215–230	<0.3	2.9	0.07	450
PPS	120	285	~0.4	2.8	0.03	500
PEN	~125	265	~0.4	~3	0.40	500

common capacitor dielectrics. The two most common capacitor film dielectrics are PET, which is available in sub-micron thickness, and BOPP, for which the minimum thickness is about 3 μm. PET has the greater dielectric constant that is accompanied by frequency and temperature dependent loss. BOPP has very low loss and the highest breakdown field (~700 MV/m for areas in the range of 1 cm^2) of commercial capacitor films but has low dielectric constant (2.2) and requires appreciable derating at operating temperatures above about 80 °C. BOPP has the greatest energy density at breakdown (5 J/cm^3) of present capacitor films and is the most common capacitor dielectric for high energy density applications. The need for high temperature dielectrics for surface mount applications has been addressed by polyethylene naphthalate (PEN) and polyphenylene sulfide (PPS) dielectrics, which can withstand temperatures generated during Pb-free wave soldering. PPS is more suitable for precision applications, with very low dielectric loss and absorption, as well as excellent capacitance stability with temperature. PEN is more suitable for "general purpose" applications where precision is not essential.

1.4. Recent activities

Given the low dielectric constant and high breakdown field of BOPP, search for new polymers with increased dielectric constant may be more promising than for those with increased breakdown field. This notion has resulted in a great deal of activity in recent years, which can be grouped into three broad classes: (1) exploiting the attractive features of polar polymers such as polyvinylidene fluoride (PVDF) and its variants [5–11], (2) multilayer capacitors in which more than one dielectric layer (of different polymer types) are placed between electrodes [12–16], and (3) filling a polymer with high dielectric constant particles or nanoparticles [17–25]. While each approach provides some benefit, all such attempts along these lines have suffered from certain drawbacks. The dielectric losses of PVDF and its variants are high while the breakdown field of filled polymers is low. The multilayer film approach offers the flexibility to mix dielectrics in ways that may be beneficial. Still, concerns related to this technology remain and center on manufacturing cost (line speed) and dielectric performance (over single layer dielectrics) for applications to metalized film capacitors. Overall, no system based on these concepts provides a clear benefit over the present materials over a wide range of applications. Each of these three material classes is discussed in some detail in Section 3.

1.5. Rational computation-driven searches for higher energy density dielectrics

The advent of computational methods provides the opportunity to *search* for novel dielectrics at reasonable cost [26–28], which extends significantly the reach of purely empirical Edisonian attempts at materials discovery. Modern computational methods have evolved from merely supporting and explaining measurements in a *post hoc* manner to guiding the design of new materials, provided methodologies are available to compute properties of interest. These strategies, when combined synergistically with experimental synthesis and characterization, provide complementary information that can accelerate initial screening and identification of promising candidates. At the most fundamental level, computational quantum mechanics, e.g., density functional theory (DFT) [29,30], can be used to determine properties of dielectrics at the scale of a crystalline unit cell [31]. Such properties include the physical and electronic structure, dielectric constant, thermodynamic stability, and intrinsic breakdown field [26,27,32–39]. In addition, impurity states in the band gap caused by typical chemical impurities and charge injection barriers at metal–polymer interfaces can be computed under somewhat idealized conditions [40–43]. Larger scale morphological features of polymers can be accessed at the present time only using molecular dynamics (MD) simulations based on empirical inter-atomic potentials or force fields [44–47]. Such simulations can predict crystal structure, semicrystalline morphology and provide rough estimates of glass transition temperature and dielectric loss, although the latter is presently limited to the GHz range [48–51]. In addition, an emerging class of methods, often referred to as "data-driven", use various forms of multivariate analysis on experimental or computational data based on variables with a physical relationship to the properties being predicted [52–56]. Such systems are "trained" on available data and then used to predict properties of interest for polymers for which data are not available. These methods can be used to search for materials with attractive properties within a chemical subspace, and, in some cases, may provide the only option to predict properties for which no fundamental approach is available (such as glass transition temperature and melting temperature).

1.6. This review in a nutshell

The primary objectives of this review are two-fold. First, we attempt to provide an overview of the present state-of-the-art pertaining to capacitor dielectrics appropriate for high energy density applications. Second, we (hopefully) provide the community with a balanced view of the challenges and opportunities surrounding capacitor material development/discovery in a practical context, including the importance of synergy between experimental and emerging computational approaches. Thus this review should allow a new researcher (e.g., a graduate student or a practicing engineer) entering the field to obtain a snapshot of various critical aspects of this emerging field in one comprehensive narrative.

The rest of this manuscript is organized as follows. Section 2 is devoted to several essential properties and phenomena that are relevant to high energy density polymeric capacitor dielectrics. In particular, this section will cover dielectric properties, electronic properties, dielectric degradation/aging, structural morphology, issues related to film formation and rheology, the metal/polymer interface, and capacitor performance. The flow presented in Fig. 3 is followed in this discussion as we move from fundamental to more practical property/behavior classes that are used to evaluate capacitor materials.

The relevance of each property or phenomena is discussed, and the present experimental and computational state-of-the-art for characterizing the property/phenomena is described in detail. Gaps in the present state-of-the-art are also discussed. Throughout the discussion in this section, attention is focused on the "standard" polymer dielectric materials used in capacitor applications. Section 3 describes some of the recently considered materials, including PVDF-based dielectrics, multilayer dielectrics, nanocomposite dielectrics, and functionalized polyolefins, while Section 4 discusses emerging large scale computation-driven search strategies that have revealed new organic and organometallic polymer dielectrics. Section 5 captures the opportunities going forward, largely with respect to required computational and experimental methodology development.

2. Key properties of polymeric dielectrics

2.1. Dielectric properties

Given that the electrostatic energy density of a linear dielectric is given by $\frac{1}{2}\varepsilon E^2$, the dielectric permittivity ε and the greatest electric field to which the dielectric can be subjected during service are important quantities. Since maximum service field is a function of application, the breakdown field of a dielectric, E_{bd}, is often used as a proxy, although E_{bd} is a function of the voltage waveform and sample area, both of which should be specified. We therefore begin our discussion with these basic of dielectric material properties, before moving on to more practical aspects that may make a particular capacitor dielectric attractive.

2.1.1. Real part of the dielectric permittivity (or the dielectric constant)

Mathematically, the macroscopic dielectric tensor $\boldsymbol{\epsilon}$ is a frequency-dependent complex quantity that describes the polarization response of a solid insulator to the presence of an external electric field $\boldsymbol{E}$, i.e., $\epsilon_0\boldsymbol{\epsilon}\boldsymbol{E} = \epsilon_0\boldsymbol{E} + \boldsymbol{P}$ where $\boldsymbol{P}$ is the polarization and ϵ_0 is the vacuum permittivity. The dielectric permittivity comes in two parts. The real part of $\boldsymbol{\epsilon}$ is related to the energy stored, while the imaginary part is a measure of dielectric loss (the ratio of the real to the imaginary parts is referred to as the loss tangent). For an isotropic material, the off-diagonal elements of $\boldsymbol{\epsilon}$ vanish while the diagonal elements are equal. In an anisotropic polycrystalline material (which may be viewed as isotropic at the macroscopic scale), the orientational average of the dielectric permittivity is the average of the diagonal elements of $\boldsymbol{\epsilon}$.

The polarization response of a solid material to an external field is not instantaneous but occurs after some delay. Under an AC field, this delay, or "friction", manifests as loss and is captured by treating the dielectric permittivity as a complex quantity $\boldsymbol{\epsilon} = \boldsymbol{\epsilon}' + i\boldsymbol{\epsilon}''$ with the loss related to the imaginary part (other sources of loss are separately discussed later). The dielectric permittivity can be measured experimentally over a wide range of frequency by dielectric (or impedance) spectroscopy. Computational methods are also available to compute $\boldsymbol{\epsilon}$ accurately, but only under specific situations as discussed in the latter part of this section. Such computational capabilities can be used to screen dielectrics. Indeed, this approach (i.e., searching for materials with high dielectric constant) has dominated computation-driven dielectrics design attempts in the recent past [26,27,32,33,57,34–36].

We first consider the real part of $\boldsymbol{\epsilon}(\omega)$ (where ω is the frequency) whose components are given by,

$$\epsilon'_{\alpha\beta}(\omega) = 1 + 4\pi\frac{\partial P_\alpha}{\partial E_\beta} + \frac{4\pi}{\Omega_0}\sum_m \frac{S_{m\alpha\beta}}{\omega^2_{m,\mathbf{q}=0} - \omega^2}. \quad (1)$$

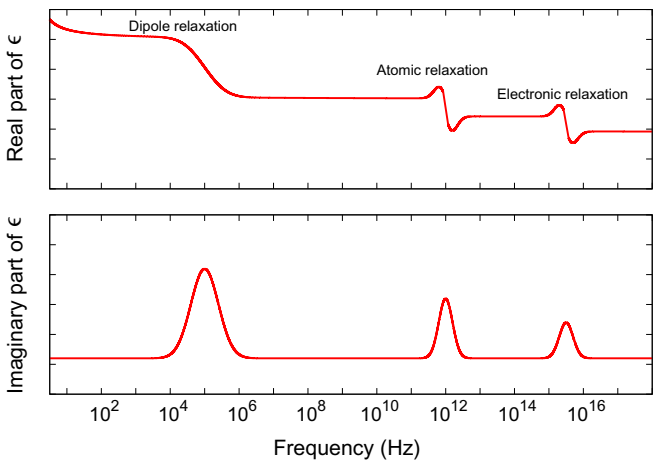

Fig. 4. Schematic of the real and imaginary parts of the orientationally averaged dielectric permittivity. The electronic relaxation is connected to the electronic part of the dielectric constant.

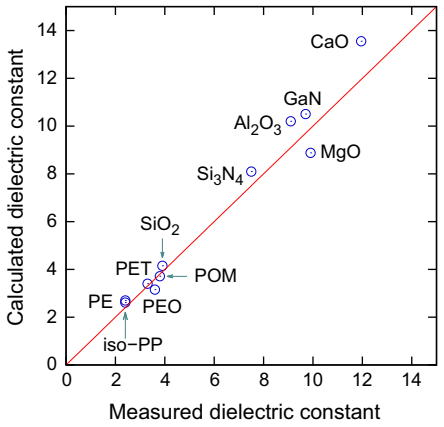

Fig. 5. Calculated and measured dielectric constants of some typical materials, including binary compounds and polymers, i.e., polyethylene (PE), poly (ethylene oxide) (PEO), polyethylene terephthalate (PET), polyoxymethylene (POM), and isotactic polypropylene (iso-PP).

Here, the first two terms comprise the electronic part and the last term describes the ionic part of the dielectric response. In the last term, Ω_0 is the volume of the unit cell of the single crystal material under consideration, which acts as the normalization factor for the sum taken over all infrared active phonon modes, indexed by m. $\omega_{m,\mathbf{q}=0}$ is the phonon frequency at the Γ point ($\mathbf{q} = 0$), i.e., the center of the first Brillouin zone, and $S_{m\alpha\beta}$ is the mode oscillator strength defined though the Born mode-effective charges. In principle, the ionic part of the dielectric response can include bond stretching motions (occurring at THz frequencies) as well as bond rotations, i.e., dipole rotations (occurring at GHz frequencies). In the case of polymers, relaxation processes occur at much lower frequencies (kHz–MHz frequencies) as a result of long timescale chain movements which cause resonances in the dielectric spectrum that are shown schematically in Fig. 4. In the following, for ease of discussion, we consider just the orientational average ϵ of the permittivity tensor $\epsilon'_{\alpha\beta}$, which is related to the *absolute* dielectric constant ε as $\epsilon \equiv \varepsilon/\epsilon_0$.

At frequencies close to optical that are well above the bond stretching and bond rotation frequencies, the last term in Eq. (1) drops to zero, and the dielectric permittivity is caused by the electronic response. This is termed as the optical or the electronic part of the dielectric permittivity, ϵ_{elec}. At low (i.e., in the limit of zero) frequencies, called the static limit, both the electronic and ionic parts contribute to the dielectric response which is denoted here as ϵ_{ionic}. The state-of-the-art method used to compute both ϵ_{elec} and ϵ_{ionic} (and hence the total permittivity, $\epsilon = \epsilon_{\text{elec}} + \epsilon_{\text{ionic}}$) is the DFT perturbation [31], which provides a good estimate of the total dielectric constant, ϵ, as shown in Fig. 5. This figure presents the total static dielectric constant of some materials, including binary compounds and common polymers, computed at the limit $\omega \to 0$ using the *Vienna Ab-initio Simulation Package* [58,59], a widely used DFT code. As can be seen, the calculated data are in good agreement with the measured data, implying that this computational technique can be used effectively to study dielectrics [26,27,32,33,57,34–36].

When morphology is important, larger scale computations can be carried out based on MD simulations using empirical force fields (when available), and the dipole–dipole autocorrelation function is used to extract ϵ_{ionic}. Although ϵ_{elec} cannot be obtained from an MD computation, it depends little on morphological aspects and can be obtained from a DFT computation.

2.1.2. Imaginary part of the dielectric permittivity (or the "intrinsic" loss tangent)

While the real part of the dielectric permittivity can be computed with reasonable accuracy, this is not the case for the imaginary part. Fig. 4 indicates schematically resonances in the dielectric response that are expected as a result of electronic, bond stretching, bond rotation and longer timescale relaxation. These resonances correspond to peaks in the imaginary part of the permittivity, and hence, peaks in the dielectric loss. Dipolar relaxation is a major contributor to dielectric loss in polar dielectrics and tends to occur below MHz. Dipoles in polar dielectrics reorient to a greater or lesser degree in response to an alternating electric field. Inevitably in a solid, such dipoles suffer from some friction with the polymer matrix which impedes their reorientation in response to change in electric field, so that the reorientation process can be characterized by a time constant or a distribution of time constants. When the frequency of the applied field causes a dipole to oscillate 45° out of phase with the electric field, the dipole-induced dielectric loss is maximized, which causes a "dispersion" peak in the dielectric loss. With increased temperature, the viscosity of a polymer usually decreases, which decreases the reorientational time constant and increases the frequency of a dispersion peak.

As a result of the low frequencies (below MHz) and the corresponding large timescales (above microseconds) involved, capturing such losses using DFT computations is not practical at present. Hence, one resorts to MD simulations using empirical force fields. Based on present computational capabilities, even these schemes can barely access frequencies in the MHz range. For example, a typical MD simulation can access, at most, 1 μs, making it barely useful in this context. While simulations can be performed on more coarse-grained models to perform "scale bridging" into the timescales (or frequencies) of interest, these do not include the necessary chemical detail for accurate estimates of the dielectric loss spectrum. At present,

the most promising approach appears to be based on the empirical time–temperature superposition principle to aid in this process [60]. This principle assumes that the system has one local relaxation process that is shifted to higher (lower) frequency with increasing (decreasing) temperature. This assumption is applicable to many classes of polymers used for dielectric applications for which the operating temperature is greater than $\approx 1.2T_g$ (where T_g is the glass transition temperature of the polymer). Boyd [61] and Müller-Plathe [62] have used these simplifications to calculate the dielectric relaxation function (whose Fourier transform yields the frequency-dependent storage and loss modulii) across a broad range of temperatures for some simple polymers, such as polystyrene. The outstanding issues are the applicability of these concepts to broader classes of polymers, and the ability of these methods to reproduce (and eventually replace) experiments for predicting the dielectric loss spectrum.

2.1.3. Dielectric absorption and conduction loss

Dielectric losses can also arise from other sources. When an electric potential is applied across a capacitor dielectric, a small amount of charge flows from the electrodes into the dielectric over time. If the capacitor is shorted for a short time (say, 1 s) and left open circuit thereafter, a voltage develops across the capacitor as a result of charge coming out of the dielectric and onto its electrodes. This dielectric absorption phenomenon is caused by several factors, including Maxwell–Wagner polarization in an inhomogeneous (e.g., semicrystalline) dielectric, filling of shallow impurity states or traps (more about this later) within the band gap, etc. Lowest dielectric absorption is found in amorphous, nonpolar dielectrics such as polystyrene and Teflon. Dielectric absorption contributes to dielectric loss and is of concern in precision analog applications but less so in high voltage applications.

Conduction is another source of loss. At room temperature, the effect of electrical conduction is negligible for most capacitors. However, the conductivity of an unfilled solid dielectric often increases by an order of magnitude every 10–20 K, following an Arrhenius relationship with an activation energy in the range of 0.5–1.5 eV. At elevated temperatures, conduction can be important or even limit the useful temperature range of a dielectric. The dielectric loss tangent includes a term $\sigma(E,T)/\varepsilon\omega$ where $\sigma(E,T)$ is the field and temperature dependent conductivity. As a result of the inverse dependence on frequency, this term always dominates dielectric loss at sufficiently low frequency and provides a method for determining conductivity.

For many bulk polymers and some capacitor films, hopping, by which charged carriers (electrons) hop between "traps", appears to dominate carrier mobility [63]. At low electric field (<10 MV/m for many polymers), carrier mobility is thermally activated, as the energy gained between traps is small compared to thermal energy, and conduction is Ohmic. When the energy gained from the electric field as a carrier moves between traps becomes comparable (about 10 MV/m and above for many polymers) with the thermal energy, it contributes appreciably to the detrapping process, resulting to a roughly exponential increase of the conductivity with the electric field. For BOPP, the transition from Ohmic to nonlinear conduction appears to be in the range of 100 MV/m [63]. When the electric field is sufficient high, the energy gained between traps approaches the trap depth and activates the trapped carriers. At this point, aging process is very rapid, and the polymers and insulators are in the pre-breakdown regime. This condition is also discussed as below. To first order, the effect of field and temperature on conductivity appears to be multiplicative and of the general form

$$\sigma(E,T) = \frac{A}{|E|^n}\exp\left(-\frac{q\gamma}{k_B T}\right)\sinh(B|E|^n) \approx C\exp\left(-\frac{q\gamma}{k_B T}\right)\exp(B|E|^n) \tag{2}$$

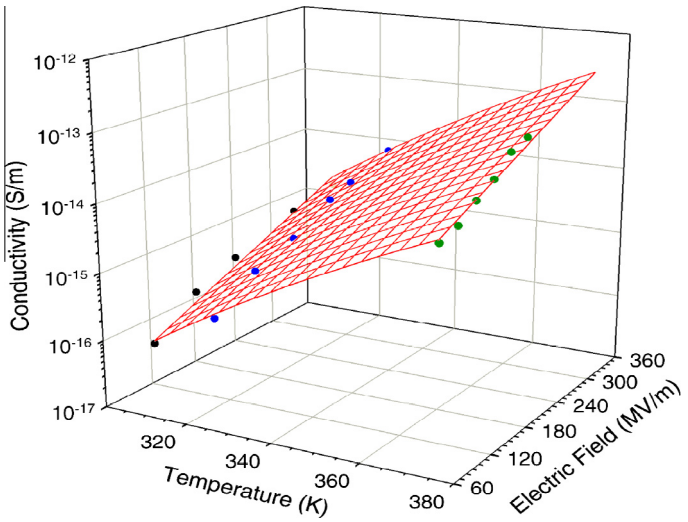

Fig. 6. Fit to measured conductivity as a function of field and temperature for 7 μm BOPP based the approximation in Eq. (2) with $n = 1$, which results in an activation energy of 0.75 eV which is independent of field. Figure taken from Ref. [63] with permission from IEEE.

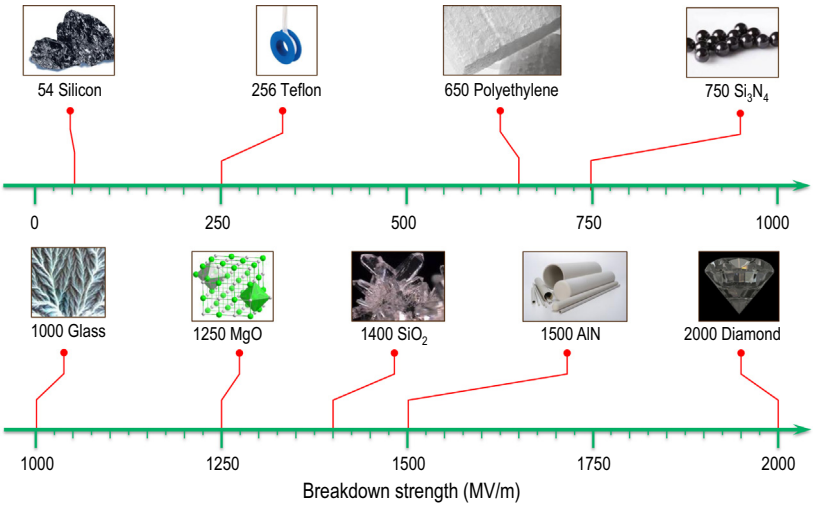

Fig. 7. The highest recorded breakdown field for several technologically important materials.

Table 2
Summary of the theories of intrinsic breakdown.

Year	Contributor	Materials	References
1932	von Hippel	Alkali halides	[65]
1934	Zener	1-Dimensional lattice	[66]
1937	Fröhlich	Alkali halides	[67–69]
1981	Sparks et al.	Alkali halides	[70]
1986	Cartier et al.	Organic dielectrics (n-$C_{36}H_{74}$)	[71]
1994	Arnold et al.	SiO_2 thin films	[64]
2012	Sun et al.	Covalent and ionic solids	[37,38]

where γ is the thermal activation energy of conduction (eV), q is the electronic charge (C), and k_B is Boltzmann's constant (the approximation in the above expression holds at high frequencies). The other parameters are constants with n often 1 or ½. Measurements of the conductivity of BOPP are shown in Fig. 6, demonstrating Eq. (2).

In the case of polar polymers, a peak in dielectric loss usually occurs at a glass transition temperature (T_g). Thus for such polymers, T_g is relevant and ideally should fall outside the operating temperature range of the dielectric. T_g is also relevant to film processing.

2.1.4. Dielectric breakdown field – general background

Since the maximum electrostatic energy density is achieved at the breakdown field, E_{bd}, and because the energy density scales with the square of the electric field, the breakdown field is clearly important. Any dielectric will break down at sufficiently high electric field, which can be caused by electron avalanche, thermal runaway, etc. In very broad terms, dielectric breakdown field tends to decrease with sample thickness for a bulk dielectric, with increased dielectric constant, with reduced hardness, etc. Breakdown of engineering polymer films depends largely on extrinsic factors such as chemical impurities, which create impurity states in the band gap (to be discussed separately later). As a result, the dielectric breakdown field of engineering materials is very difficult to predict and depends on many extrinsic factors such as surface roughness, quality of manufacturing, and quality of raw materials. Before we delve into the intricacies of such extrinsic factors, we provide a concise description of *intrinsic* breakdown.

2.1.5. Intrinsic dielectric breakdown

While the engineering breakdown field of a material is determined by a multitude of often extrinsic factors, the intrinsic breakdown field of a dielectric is the breakdown of a "perfect" material in a very short time, i.e., without the effects of dielectric aging. Intrinsic breakdown is thus determined purely by the chemistry of the material (i.e., the atoms of which the material is composed, the bonding between the atoms, and the arrangement of atoms). As a result, the intrinsic breakdown field varies greatly with band gap, phonon density of states, etc. (see, for instance, Fig. 7). The intrinsic breakdown field provides an upper bound (or the theoretical limit) to the engineering breakdown. The measurement of intrinsic breakdown is always problematic, as "perfection", even in crystalline materials, is difficult to achieve on a macroscopic basis. Electrode–material interfaces are never perfect, and, in principle, the position of the electrode Fermi level within the band gap and relative to impurity states can affect the breakdown field. Thus when metallic electrodes are employed, many tests must be carried out,

and the intrinsic breakdown field is taken as the upper limit of the experimental data. More recently, intrinsic breakdown has been measured using an intense optical field, which, for transparent materials, avoids electrode effects [64].

Since the intrinsic breakdown is a material property, it is computable, as it is determined purely by the chemistry of the material, i.e., the elements the material is composed of, the atomic-level structure, and the bonding. The story of the theory of intrinsic dielectric breakdown starts around 1930, when researchers such as von Hippel, Zener, and Fröhlich started to explain electrical breakdown, first using semi-classical theories and eventually using quantum mechanics. The essence of the theory is that breakdown occurs when the electric field is sufficiently large that electrons in the high energy tail of the electron energy distribution, which have sufficient energy to cause impact ionization, gain more energy from the field than they lose to phonons. A historical and semi-technical description of the refinements of this theory from the 1930s to modern times (culminating in a DFT based implementation) has been described recently [38], and is captured in Table 2.

The ability of modern quantum mechanical methods to calculate the electron–phonon scattering rates [72–74] has provided the basis to compute quantitatively the intrinsic breakdown field of any material [37]. Following Fröhlich's original ideas, most theories of intrinsic breakdown start from the hypothesis of an electron avalanche at the intrinsic breakdown field. A central tenet of this theory is that electron–phonon interactions provide the only relevant scattering mechanism for charge carriers. Electrons gain energy from an external electric field between collisions with phonons. At low electric fields, the electron energy distribution achieves steady state, as the energy gain from the external electric field is balanced by energy loss from collisions with phonons. At a sufficiently high electric field, the electron energy increases indefinitely until a threshold is reached at which a high-energy electron ionizes the lattice, leading to carrier multiplication. This process is referred to as impact ionization, and the ensuing avalanche of electrons can damage the material (e.g., through bond breakage). Within this framework, the breakdown criterion can be formulated as the lowest field at which the average electron energy gain from the field is greater than the average energy loss to phonons.

While quantum mechanical descriptions of intrinsic breakdown are well over 70 years old, until recently, the estimation of the relevant parameters, such as the electron–phonon coupling function, has relied on approximations or empirical deformation potentials [75–77]. Recent work in which the electron–phonon coupling function is computed from first principles using density functional perturbation theory (DFPT) [31] has provided a first-ever generally applicable approach [37] to the computation of intrinsic breakdown for a wide variety of insulators [37,39]. Computed data are compared to the best available experimental data in Fig. 8. As can be seen, the favorable agreement between calculations and experiments spans two orders of magnitude in the breakdown field. While these calculations are time-intensive and require optimization, the framework is now available to determine the intrinsic dielectric breakdown field of any insulator from first principles, which paves the way for purely computation based initial-level screening of high electric field tolerant materials.

2.1.6. Engineering breakdown

Most engineering dielectric materials are composites (e.g., oil–paper, SF_6-polypropylene film, etc.), polymers, liquids, or gases. Gas breakdown is well understood on the basis of field-dependent, collisionally induced carrier generation, attachment (in the case of electronegative species) and detachment. Under well-controlled conditions, the threshold field for breakdown of gases is extremely sharp. In engineering situations, cosmic ray-induced carriers in the gas can affect the statistics of breakdown, especially for electronegative gases (e.g., SF_6) under transient conditions. Under inhomogeneous

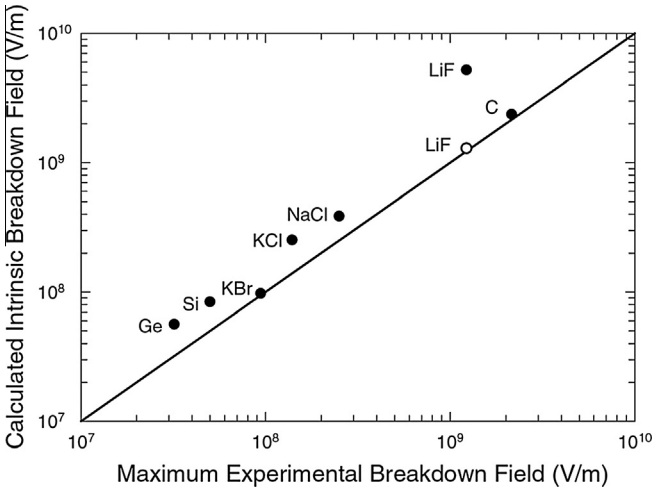

Fig. 8. Maximum experimental breakdown field versus the calculated intrinsic value [37] for a range of covalent and ionic materials. In the case of LiF, the enthalpy of formation (6.39 eV) is much lower than the band gap (14.2 eV). Bond breakage will thus occur before impact ionization. The open circle in this case is the result when the formation enthalpy is used in the calculations instead of the band gap. Figure reprinted from Ref. [37] with permission from AIP Publishing.

field conditions, gas breakdown often takes place in a step-wise manner, which can take 100s of ns to cross a gap of some cm [78].

Breakdown in liquids and solids is complicated by the fact that ultimate (avalanche) breakdown only occurs in a gas. Thus a gas channel must form within the liquid or solid prior to catastrophic breakdown. In the case of intrinsic breakdown, this occurs in a single step within a very short time. Under most engineering conditions, the precursors to breakdown can develop over anything from nanoseconds to years, and the phenomena of greatest concern are usually those which develop over longer periods of time. Liquid breakdown is a very complex subject which involves bubble formation, carrier multiplication, and extension to form a gas channel within the liquid, the details of which vary with the field inhomogeneity, applied voltage risetime, and voltage magnitude. The interested reader is referred to review articles on the subject [79,80].

Solid breakdown differs from liquid in the lack of constituent mobility, so that long-term, progressive damage is possible as damage is local and immobile. This does not change the underlying mechanisms as much as it changes the time scale over which breakdown can develop. Under AC or repetitive transient conditions, a "dangerous" field enhancement in a solid dielectric results in cyclic charge injection of alternating polarity and development of a space charge limited field region (SCLF) in the high field region of the system. Alternating polarity charge injection can also occur for a series of unipolar pulses [81]. The SCLF is the result of the field-dependent conduction which limits the electric field through space charge formation. Under AC conditions, the SCLF, E_{SCLF}, is determined by the condition that $\sigma(E_{SCLF}) = \varepsilon\omega$ where σ is conductivity, ε is the material absolute dielectric constant, and ω is radial frequency of the applied voltage which can also be taken as the inverse of a voltage transient rise time. Under AC conditions, positive and negative space charge cycle within the SCLF region, which results in UV photons and excitons generated by carrier recombination, both of which degrade the solid [81]. Eventually this degradation weakens the solid to the point that field-induced mechanical stresses cause the material to yield to form a cavity in which gas discharge can occur which, over time, results in growth of dendritic gas-filled channels which lead to breakdown. The initiation of such channels is generally more difficult than their growth once initiated, so the limiting factor for eventual failure is the formation of an SCLF region of sufficient extent in the direction of the field (a few μm) to initiate such channels [82]. The time scale for failure by this mechanism, generally referred to as "electrical treeing", is seconds to decades.

In bulk solids, high fields are limited to a microscopic region around a field enhancement region, as the power density in such a region would cause thermal failure on a larger scale. For thin polymeric films, such as capacitor films, similar phenomena are likely to occur at the high fields to which they are exposed, as evidenced by light emission from such films with spectral evidence of exciton formation [83]. In this case, the field enhancement is much less, but the film is so thin that exciton formation, bond cleavage, resulting formation of impurity states such as carbonyl, and enhanced conductivity therefrom are likely to result in positive feedback leading to local breakdown. In the case of BOPP, for example, breakdown in air typically occurs in less than an hour at about 70% of short-term breakdown. In an anaerobic environment or impregnated with an appropriate liquid, the film is more stable. These phenomena suggest, as is well known for bulk solids, that high field degradation in the presence of oxygen is much more rapid than in a more benign environment (vacuum, N_2, etc.). Carbonyl is also known to cause impurity states in many olefinic polymers, which often enhance bulk conduction, most likely by increasing hole mobility. If, on the other hand, such impurity states fell within the valence band or conduction band, their detrimental effect might be negligible.

A great deal has been written on "mechanisms of breakdown" (thermal, mechanical, etc.). However, in the "real world" of engineering, this subject is much less important than the underlying physics and chemistry of high field degradation.

2.1.7. Measurement of dielectric breakdown field

Procedures for measuring film breakdown properties are well described in the literature, and several automated instruments for measuring breakdown of capacitor film have been developed [84]. The breakdown field of a large area semicrystalline film (area of the order of m^2 in the case of an electrostatic energy storage capacitor) is limited by film morphology and the large area statistics thereof across a thin film, the statistics of film surface roughness and the field enhancements caused thereby, etc. Dielectric breakdown, as an example of a "weakest link" problem, generally fits a Weibull distribution or, less often, a log-normal distribution. The Weibull characteristic breakdown field, η_1, varies with area, A, as

$$\eta_1 = \eta_0 \left(\frac{A_0}{A_1}\right)^{\frac{1}{\beta}} \tag{3}$$

where η_0 is the breakdown field corresponding to the initial area A_0, with η_1 the extrapolated breakdown field at area A_1. The Weibull slope parameter, β, for the breakdown field of well-manufactured commercial film is in the range of 20, which indicates a relatively narrow distribution. Thus to preserve high breakdown over a large area, large β is essential, and for breakdown measurements to be meaningful in an absolute sense, an active area must be specified along with η and β.

2.2. Electronic properties

2.2.1. The band gap

The electronic band gap is a good measure of the quality of an insulator, with larger values correlating to impressive insulators (such as polyethylene or SiO_2, with band gap larger than 8 eV) and smaller values associated with systems that can be

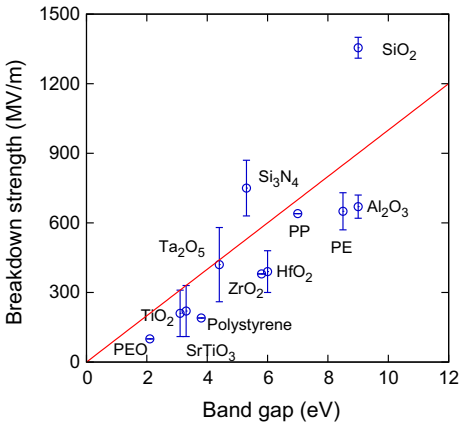

Fig. 9. Breakdown field vs. band gap. Data used for this figure was taken from Ref. [85] with errorbars representing the fluctuations in various independent measurements. The red line tentatively sketches the correlation between the breakdown strength and the band gap.

conductive when doped (such as polyacetylene and Si, with band gap in the range of 1 eV). Nevertheless, the role of defects, impurities and imperfections, cannot be understated. These entities are inevitable in real materials, and lead to occupied or unoccupied electronic states in the band gap, which can aid conduction, contribute to dielectric loss, catalyze further damage, and, ultimately, lead to breakdown (ideally, if such defect states fall outside the band gap, their negative effect is expected to minimal). Empirical evidence, as captured in Fig. 9, suggests that the band gap is roughly correlated with the breakdown strength. Thus, although defects and imperfections are indeed important, tracking the band gap of dielectrics can serve as an important initial screening aid during materials selection, as has been demonstrated in the past within the context of the search for "high-k" dielectrics in the microelectronics industry [85], and more recently, in searches of polymer dielectrics for capacitor dielectrics [26,27,32–36].

Experimentally, the band gap can be determined either by photoemission or photoconduction spectroscopies. The quantity obtained can differ from that derived using optical absorption, as the latter can involve creation of either excitons or electron–hole pairs. In the case of PE, for example, the band gap obtained from photoconduction (8.8 eV) is over 1 eV greater than the threshold for electronic absorption (7.6 eV) as a result of exciton creation (the latter can then excite electrons from the gap states) [86,87]. In practice, measurements are routinely based on ultraviolet–visible (UV–Vis) photoelectron spectroscopy, although constraints remain related to the vacuum environment, UV sources, possible degradation and charging of materials, and the fact that it is essentially a surface analysis [88]. Band gap measurement for experimental samples may be complicated by presence of impurities (that cause defect states). Examples of UV–Vis transmission spectra of PE and PET that show band edge and absorption caused by impurities are given in [89]. Nevertheless, experimental techniques are available to measure band gap (or even the entire band structure).

Accurate computation of band gap remains problematic. Within the framework of DFT, the band gap of an insulator is determined by finding the difference between the energies of the lowest unoccupied state and the highest occupied state of the band structure. This conventional approach generally underestimates the predicted band gap with respect to experiments by 30% or more as a result of approximations made to represent the quantum mechanical exchange–correlation interaction between electrons [90]. The most common such approximations include the local density approximation or the (semi-local) generalized gradient approximation (GGA) functionals. However, the shape and the width of the bands, and trends in changes in the band gap (e.g., due to external pressure) are predicted accurately [91]. Better estimates of the band gap can be achieved using a range of more computationally intensive methods, many of which are gradually becoming computationally more affordable as the cost to processor speed ratio decreases. One such method involves usage of "hybrid" functionals in which a part of the approximate GGA exchange energy is replaced by the exact non-local exchange energy obtained from a Hartree–Fock-like theory. A commonly used hybrid functional for this purpose is that developed by Heyd, Scuseria, and Ernzerhof (HSE) [92], which improves significantly the band gap estimation over data based on GGA. In a more sophisticated method referred to as GW theory [93–95], the insulator band gap is determined based on the excitation spectrum of the system upon removal or addition of an electron. This problem is treated within the many-body perturbation theory involving the single-electron Green function and electron self-energy, and typically provides very good agreement with the experimentally determined band gap of insulators. In Fig. 10, the performance of HSE and GW theory is contrasted with the conventional GGA functional. Such advanced methods are used in recent computation-driven searches of polymeric dielectrics for high energy density applications [26,27,32–36,57].

2.2.2. Experimental characterization of defects and imperfections

Defects and imperfections can occur in many forms and scales in dielectrics, ranging from physical disorder, (e.g., deviations from the crystallinity), to chemical defects (unexpected/undesired functional groups, e.g., carbonyls in PE), and voids at the micro- or macroscopic scales. Atomic-level imperfections, i.e., physical and chemical defects, can impact directly the

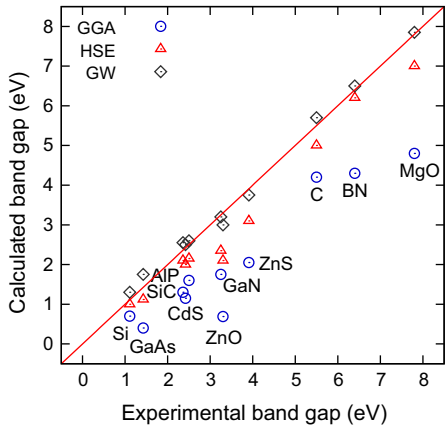

Fig. 10. Comparison of the calculated electronic band gap (at various levels of theory) of a variety of insulators with the corresponding experimental values.

electronic structure and the electrical performance of dielectrics by introducing defect states within the dielectric band gap which can act as trap centers and sources of charge carriers. Defect states can increase carrier mobility, leading, at high electric fields, to a positive feedback mechanism that increases the defect state density which increases local carrier mobility to cause high field aging and eventual breakdown [96,97]. On the other hand, micro- and macroscopic imperfections lead to electric field enhancement, which can promote creation of chemical defects.

The presence and the nature of chemical defects in polymer dielectrics is best investigated using a variety of luminescence measurements, including photoluminescence (PL), electroluminescence (EL), charge recombination-induced luminescence (RIL) [98], thermoluminescence (TL), and cathodoluminescence (CL). Defects, depending on their type and the energetic placement of their defect levels, play differing roles in these luminescence diagnoses. PL is dominated by intra-defect transitions, i.e., those that occur between the electronic states of the same defect. EL and TL, on the other hand, typically involve the intra-defect transitions and transitions between the defect levels and either the valence-band maximum (VBM) or the conduction band minimum (CBM), i.e., the charge recombination processes [83]. These transitions lead to characteristic emissions that can be used to identify a range of defects in PE, e.g., carbonyl, dienone, vinyl, and hydroxyl [99,100]. The luminescence measurements can also provide information regarding the degradation of polymers [83] and can be used to probe electrically active defects, i.e., those that constitute traps for storing and releasing energy upon recombination, and the chemical processes that involve defect excited states.

Probably the most common luminescence technique is PL, which provides access to optically active chemical defects in the absence of an electric field or charge transport. In RIL, traps are identified by making them active, e.g., by "charging" them and examining energy release signatures. If a charge recombination process can be made to release energy only through light emission, the resulting luminescence provides a unique signature related to the nature of the traps. PL can be used to probe chemical defects and residues [101]. Despite its sensitivity, a number of challenges remain. First, assignment of the emission bands is never straightforward as no tabulated spectroscopic data are available, and the emission properties of a given molecular species depend largely on its environment, e.g., polarity and local density [102]. Second, the sensitivity of these techniques depends strongly on the nature of the defects, e.g., detecting aromatic moieties is easy due to their large quantum yield, while identifying polyenes is more difficult. Third, obtaining information at the quantitative level is difficult for dense media.

Several types of luminescence processes involve materials irradiated by X-rays, γ-rays, or hard UV light [103–105]. Such excitation generates charges internally by ionization of the polymer, and these charges subsequently recombine as the sample temperature is increased. Even though these methods are intended to provide intrinsic characterization of the polymer, generating charges from an external source, as by contact with a non-reactive cold discharge at low temperature [98,100] has advantages. The resulting luminescence is characterized by time-resolved luminescence spectra (Fig. 11). Spectra obtained a few minutes after excitation switch-off are caused by the recombination of the charges previously deposited on the surface under the AC discharge. Such RIL spectra characterize phosphorescence emission, even if the photoluminescence of the material has both fluorescence and phosphorescence components. Fig. 11 shows PL and RIL spectra of benzophenone grafted cross-linked PE that exhibits specific spectral features, such as vibronic structure associated with the carbonyl function bound to aromatics.

PL can also be used to probe singlet and triplet electronic states by setting the measurement temperature appropriately, which provides further information for defect identification [107]. The issue is to determine whether triplet states of the recombination centers are excited upon charge recombination or if the phosphorescence is seen because it is the only possible radiative transition. The recorded fluorescence and phosphorescence do not necessarily correspond to the same chromophore because the transition probability can be low for one or the other relaxation pathway, depending on chemicals and surrounding medium [106].

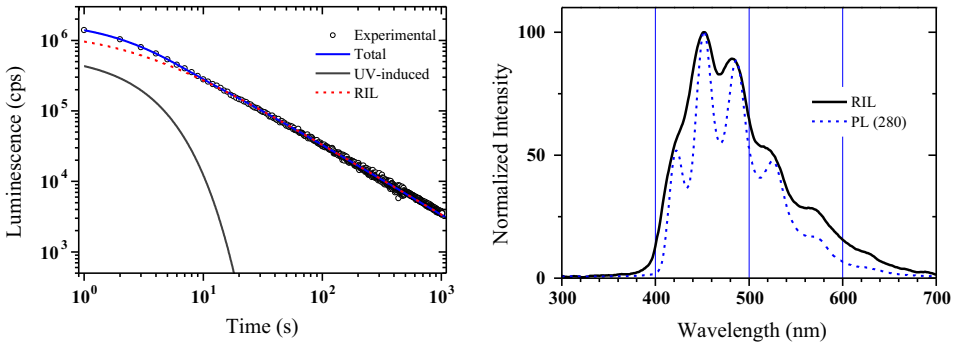

Fig. 11. (Left) Integral light decay following material excitation by a short plasma discharge. The charge recombination-induced luminescence (RIL) is the main contribution to the light decay (hyperbolic dependence in time). (Right) Photoluminescence (phosphorescence) and RIL spectra. Results obtained on PE with grafted benzophenone derivative to 1 wt.%. Figure adapted from data reported in Ref. [106].

Both EL and CL spectra are composed of several elementary spectral components, each of which originates from a given mechanism and corresponds to a characteristic wavelength. In case of PP, they are the fluorescence (the relaxation of singlet states) of natural chromophores, the CL involving the formation of carbonyl, the luminescence induced by charge recombination on chromophores, and a dominant contribution associated with some excited species that are related to polymer degradation [83]. As shown in Fig. 12, all of these components were identified [83] in both the EL and CL of PP, but with differing relative contributions. Likewise, Fig. 13 shows the signatures of carbonyl defect in PE obtained through many different luminescence measurements. The assignment of the spectral features to specific defect states is confirmed through computational work that will be discussed in the next section.

Trap depth also might be accessed using TL in which a material is subjected to an ionization source at low temperatures to trap charges within the material, after which the temperature is increased, during which carriers are released from traps to produce a current (TSC) and luminescence (TL). Analysis of the TL is performed based on direct tunneling or first order kinetics-based thermal detrapping. In principle, trap depth can be deduced as the activation energy of the TL or TSC curves [108]. The analysis is based on multiple assumptions [109], including that the process does not correspond to physical disappearance of the trap through molecular motion, that the quantum efficiency does not change with temperature, and that a single detrapping process is at play (non-distributed process) which is rarely the case in polymers.

2.2.3. Computational characterization of chemical defects

An alternate (and complementary) approach to identifying material luminescence signatures is provided through DFT and beyond-DFT computations, which have contributed to the understanding of similar phenomena in the past [110–112]. In case of polymers, such computational work is in a state of infancy and is restricted mostly to defects in PE [40,41,113–115]. Past DFT work (on PE) is based mostly on the use of (semi)local exchange–correlation GGA XC functionals. Defect states are then identified as the one-electron Kohn–Sham eigenenergies [40,41,114,115], just as the band gap is viewed as the energy difference between occupied and unoccupied one-electron levels. While this approach provides a *qualitative* picture of the defect-derived energy levels, it has several fundamental drawbacks. First, the one-electron levels computed by DFT have no physical meaning as they relate to the energy levels of a fictitious set of non-interacting "electrons" [29,30]. The

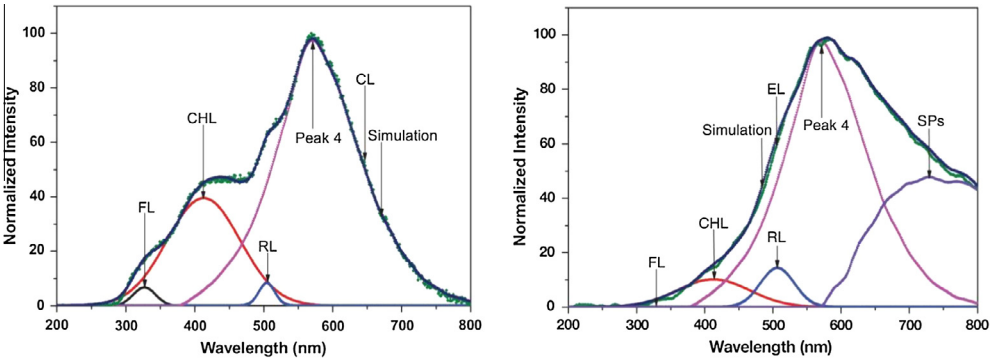

Fig. 12. The reconstructions of the measured (left) cathodoluminescence (CL) and (right) electroluminescence (EL) spectra of PP. Four components, namely fluorescence (FL), chemiluminescence (CHL), recombination-induced luminescence (RL), surface plasmons (SP). Peak 4 is assigned tentatively to some (still unknown) excited species associated with the chemical degradation of PP. Figures reprinted from Ref. [83] with permission from IOP publishing.

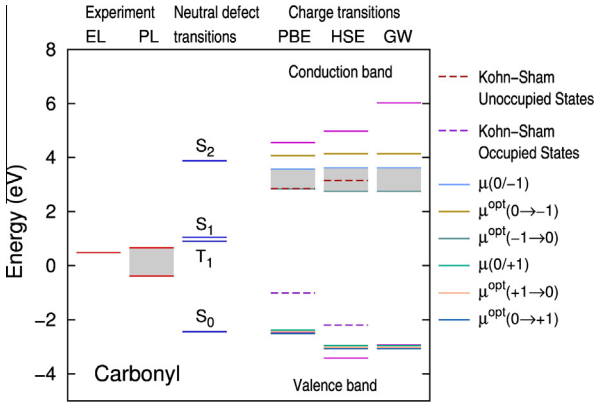

Fig. 13. Neutral defect energy levels (S_0, S_1, S_2, and T_1) among which the intra-defect state transitions take place, and charge transition levels calculated for carbonyl defect of polyethylene. Experimental (EL and PL) data are given for comparison. Figure adapted from data reported in Ref. [42].

second issue relates to the problem of computing the band gap accurately using traditional DFT, already discussed in Section 2.2.1. The significant underestimation of the calculated band gap with GGA XC functionals causes uncertainty in the location of the defect energy levels within the band gap as well as the position of the conduction and valence band edges [95,116]. Finally, intra-defect transitions, i.e., those that dominate the PL spectrum as discussed in Section 2.2.2, cannot be computed.

In recent work [42], these issues have been addressed for the case of chemical defects in PE by going beyond the single-particle picture of defect levels. Calculations for intra-defect transition energies are straightforward, based on computing the DFT energies of the defect-containing systems at their ground state (usually singlet S_0) and the excited states (singlet states S_1, S_2, etc., and triplet states T_1, etc.). Solving the other problems, i.e., those related to the defect level positions within the band gap, requires a slightly more complicated approach. In particular, charged defect levels are characterized in terms of thermodynamic and adiabatic charge transition levels (i.e., the electronic chemical potential at which the charge state switches value) that involve total energy differences of charged and neutral defect calculations. The basic premise of this approach is that total energy differences between neutral and charged states provide a formally correct and quantitatively better description of energy level differences in molecules and solids (including defect level placements) [111,112,117]. To determine accurately the band gap of PE and its conduction and valence band edge positions, hybrid HSE06 functionals and the GW scheme are used. This computational approach provides direct, quantitative access to luminescence data of PE with chemical defects. Comparison of the calculated and measured spectra of carbonyl, the most common defect in PE, is given in Fig. 13 [42]. By relating the computed charge transition levels to the measured luminescence signatures (via appropriate electron transition mechanisms), this work leads to a compelling picture of defect states in PE, e.g., that the measured PL spectral peak is caused by the $T_1 \rightarrow S_0$ transition. Further details of the computations, interpretations and comparisons with experiments for the carbonyl defect as well as for other defects can be found in [42]. The above computational procedures provide a systematic approach to determine the luminescence signatures of various pre-existing defects in PE as well as other insulators.

2.3. Dielectric degradation/aging

The previous section dealt with recognizing pre-existing defects in dielectrics, and characterizing/determining their electronic signatures. While this is an important step, unraveling *progressive* changes in the defect and trap distribution of dielectric materials as a function of time at high field in various environments is an active area of research. Both "physical" and "electrochemical" aging take place over time. "Physical aging" involves structural reorganization of the polymeric matrix and/or diffusion of chemical species, both of which impact electrical properties. Physical aging is to some degree reversible. Here we mainly consider field-assisted creation of chemical defects, which leads to irreversible modifications of the material properties as assumed in all the scenarios of "electrical" or "dielectric" aging.

2.3.1. Diagnostics for the electric field assisted creation of defects

Within this context, aging is a gradual change of state and material properties that usually leads to a degree of malfunction [118]. The primary underlying process here is the cleavage of chemical bonds, which results in reorganization of the polymer and formation of new species. Aging is related directly to the chemical kinetics of defect creation in the presence of an electrical field (here, we primarily consider DC fields). Over time, the individual atomic processes collectively give rise to microscopic and, ultimately, macroscopic, recognizable changes in the substance and its ability to function. Diagnosis of such defect creation processes is difficult as they result from the application of a high field and therefore the material is polarized (i.e. dipolar orientation) and charged (i.e. electrical charges are trapped). Relaxation can take a very long time,

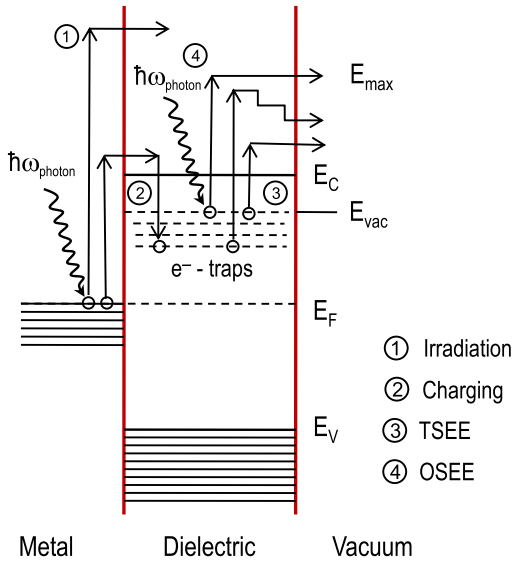

Fig. 14. Various processes involved in an exo-electron emission experiment on a thin insulating film. Processes are (1) irradiation by photo injection of hot electrons from the metal substrate; (2) charging of the overlayer by low energy electrons; (3) thermally stimulated exoelectron emission (TSEE); and (4) optically stimulated exoelectron emission (OSEE).

hours or days, and the removal of all the electrical charges is virtually impossible when charges are trapped deeply (detrapping time for a charge on a 1 eV deep trap is of the order of 400 s, and it is about 10^{10} s for a 1.5 eV deep trap [114]). As a result, differentiation between the effects of charging and impurity state formation in the band gap is difficult. Attempts at such differentiation have been based on analyzing charge decay after a period of charging in an attempt to unravel modification of the trap energy distribution caused by high field aging. This has been developed using the space charge measurement methods to quantify the amount and spatial distribution of the space charge inside the material [119,120]. The analysis involves several hypotheses and is only valid under limited conditions: thermal detrapping of carriers, transit time < trapping time, and unipolar transport. Other spectroscopies have also been used in order to unravel the trap energy distribution, including iso-thermal discharge current [121], thermo-stimulated discharge current [122], thermo-stimulated luminescence curve [123], photo-simulated discharge current [124], and exo-electron emission spectroscopy [125] as illustrated in Fig. 14.

Although some of the above methods can give information related to the nature of the defects formed, generally they are not very specific. A wealth of physical/chemical spectroscopic methods has been used to characterize field-induced defects. This is not a simple task owing to the *inhomogeneous* nature of dielectric aging that results from both initial material inhomogeneity and degradation positive feedback mechanisms. One way to deal with this difficulty is to concentrate the analysis on a small high field volume that has been stressed in the limit of the local breakdown appearing in the form of fine tree-like tubules. This is currently achieved by using "needle like electrode" under AC electrical stress where a high divergent field exists in a localized region at the tip of the needle in series with a much lower field domain to prevent thermal runaway [126]. Under these conditions, a local microprobe can be concentrated in the high field volume and Raman and Fourier Transformed Infrared spectroscopies have evidenced the increasing density of C–C bond unsaturation and carbonyls in PE and PP [127]. Other attempts to unravel changes in material properties on samples submitted to moderate field under quasi-uniform field configuration have been made using a range of spectroscopies [128]. The process of electrical aging can be tackled by detecting the evidence of the creation of excited states following the interaction between the electric field and the molecules. The most promising tool is EL which is based on the creation of highly excited states that result in light emission. Some of these states can be unstable leading to bond breaking reactions [129]. The technique is powerful in the sense that the emission is from the area subjected to a high field and prone to irreversible high field degradation. EL has been detected under many voltage waveforms above a threshold field, including DC, AC, or impulse voltage. Under DC, measurements of space charge distribution and EL combined with charge transport modeling indicate that charge recombination is a major cause of light emission which occurs in the bulk [130]. The emission is distributed relatively homogeneously in the sample plane. Modeling allows locating the recombination domains along the field direction. Under AC stress, charge recombination at the polymer–dielectric interface is a major cause of the emission [131]. Under impulse voltage, a combination of both charge recombination and hot electron effects is probable. Emission spectra are difficult to analyze due to the weakness of the emission but provide information about the species being created. Recent progress has been made in interpreting such spectra by comparing the emission features caused by various types of excitation, some of them leading to reversible effects (e.g. mild-UV PL), and some others linked to chemical reactions (e.g. CL, see Fig. 12). The EL of PP and PE films results from degradation reactions that proceed through a generic route common to both materials [83].

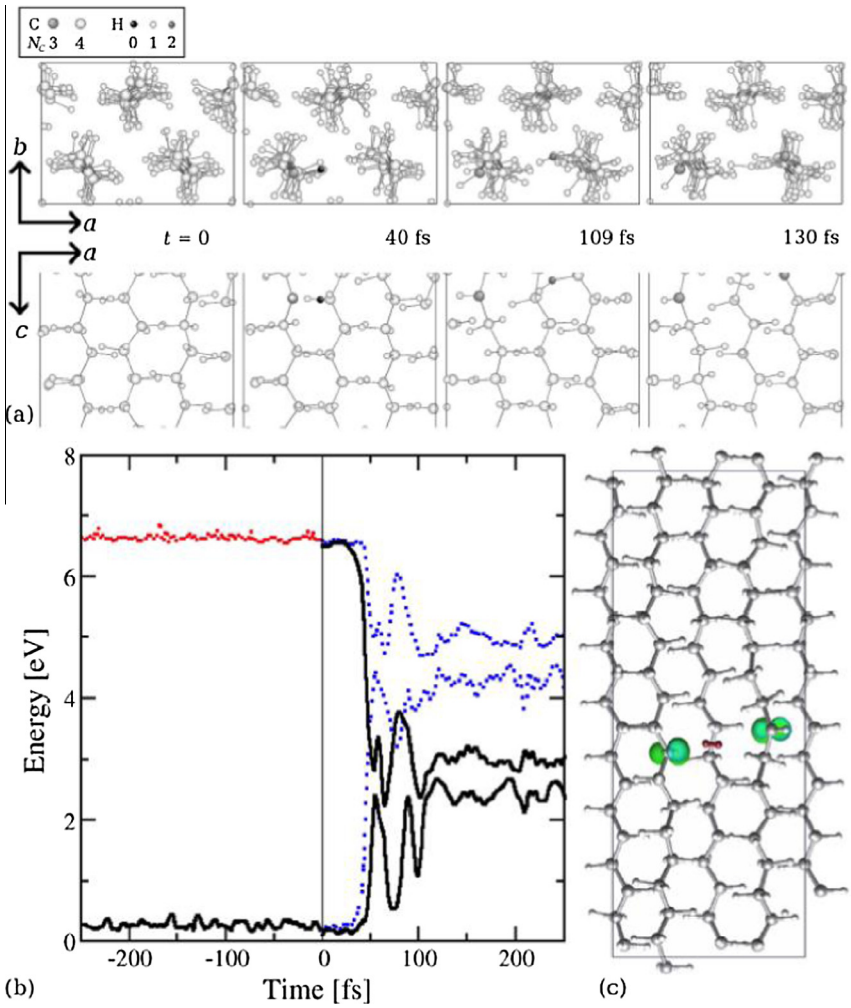

Fig. 15. Snapshots taken at time t during *ab initio* MD simulations of polyethylene (PE), where $t = 0$ refers to the point at which the exciton was injected. Atoms are shaded according to coordination number. The snapshots illustrate C–H bond scission and the subsequent H abstraction. (b) Evolution of the highest occupied and lowest unoccupied energy eigenvalues of the system for 250 fs prior to ($t < 0$) and after ($t > 0$) exciton injection. The zero of energy is the value of the highest occupied PE eigenvalue at $t = 0$. Prior to exciton injection, each of the two levels shown is doubly occupied (the colors shown correspond to spin up states). Upon triplet exciton injection, both hitherto spin-degenerate states split into an occupied spin up (full black lines) and an unoccupied spin down (dotted blue lines) state. (c) Magnetization density plot of the system at $t = 121$ fs. The magnetization is tightly localized on the –CH– groups along the main chains, indicating that these groups have unpaired electrons. The H_2 dimer is shown in deep red for clarity. Figure taken from Ref. [113] with permission from AIP Publishing.

2.3.2. Modeling the dielectric "aging" process

Atomic level understanding of dielectric aging is in its infancy, and the relationship between EL and degradation is not understood fully. A strong potential exists to link DFT based ground state, excited state and MD simulations with complementary experimental diagnostic characterization to unravel the exact nature of some EL spectral features that have not been assigned to a particular species, as well as to understand the progression of defect creation.

As must be evident from the above discussion, in addition (and due) to pre-existing defects, the electric field and temperature combine to create further defects in the dielectric. Electric field is expected to alter the materials in two ways: (1) indirectly, by creating excited states via an electron in the conduction band and a hole in the valence band; and (2) directly, by distorting polar parts of the dielectric. The former (i.e., indirect) effect can be simulated by creating excited states and monitoring how the energy generated during the recombination process causes bond cleavage and defect formation using DFT-based MD simulations. This has been carried out in the recent past for the case of PE [113]. The study assumed that electrons, holes, and excitons are present in the system (e.g., from field-induced charge injection). The key finding of this work is that the presence of triplet excitons can be damaging. The electron and hole states of the exciton localize on a distorted region of PE where they weaken nearby C–H bonds which facilitates C–H bond scission. The estimated barrier to cleavage of the weakened C–H bonds is comparable to the thermal energy, suggesting that this mechanism may be responsible for the degradation of PE under an electric field. Fig. 15 shows a snapshot of this process during the course of

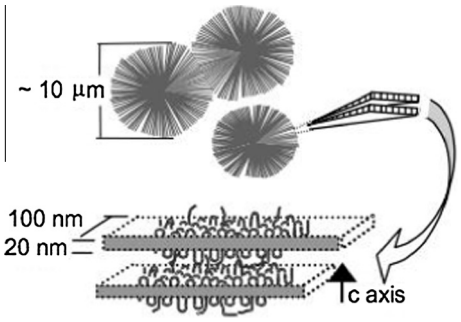

Fig. 16. Morphology of semi-crystalline PE showing spherulites composed of crystalline-amorphous ribbons. Figure reprinted from Ref. [133] with permission from IEEE.

a DFT-based MD simulation. Spectroscopic signatures associated with defect creation are in good agreement with the electroluminescence measurements by Laurent et al. [132].

Going forward, a combined experimental–computational approach will be most effective to characterizing the presence, creation, and evolution of chemical defects in polymer dielectrics as is necessary to make headway toward a comprehensive understanding of dielectric aging and degradation in the presence of a large electric field.

2.4. Role of structure/morphology

Given the central role of the [structure ↔ property ↔ processing] paradigm in materials science, the structure of polymer dielectrics is expected to be an important determinant of their dielectric behavior. This is particularly true in the case of polymer dielectrics, in which several structural scales are relevant, including crystallinity or lack thereof (and unit cell level crystalline structure if present), greater length scale features including lamellar morphology or oriented crystalline morphology, the volume fraction of the crystalline region in an amorphous matrix, and the preferential orientation of polymer chains. The morphological structure of polymer films is also influenced by the thermomechanical history during film formation. Non-crystalline materials can be melt-processable (e.g., PS, PC, etc.), or solution processable (e.g., polyimides). Melt processable polymers typically have glass transition temperatures (T_g) well above room temperature because of high stiffness of their chain backbones (BOPP is a notable exception though, which is extrudable). On the other hand, polymers which can only be solution processed are those that degrade before they melt, and are typically aromatic materials (e.g., Kapton). These materials tend to have very high T_g often in excess of 250 °C. Semicrystalline polymers, e.g., PE, PP, PET, PVDF, and certain polyimides, are melt processable. They are subdivided into two categories, i.e., fast crystallizing materials and slow crystallizing polymers. The demarcation between the two categories depends on whether the T_g is below or above room temperature from practical processing point of view. Fast crystallizing polymers like PE, PP, and PVDF typically have simple chain architectures with a great deal of flexibility, leading them to possess low T_g well below the room temperature and hence exhibit fast crystallizabilities from the melt. Polymers of the slow crystallization rate category, e.g., PET, PEN, PEEK, and certain polyimides, typically exhibit T_g well above the room temperature, even though their molecular architecture allow them to crystallize under the right conditions. They are easily quenched into glassy state. Ultimately, of course, the structural situation will determine, or contribute to, properties such as short-term breakdown field, thermal conductivity, and thermal stability.

In the case of fast crystallizing polymers such as PE, PP and PVDF, the casting stage leads to formation of semicrystalline structures. In the absence of significant deformation during casting from melt, these polymers generally exhibit spherulitic structure that is made up of radially emanating lamellae from central nuclei that are separated by amorphous regions, as shown in Fig. 16. Details of the morphology of these structures are dictated by chain architecture including branching as well as crystallization conditions. Correlations between the spherulite morphological details and electrical breakdown (mediated by Maxwell stresses) are known to exist [133].

2.4.1. Relevance to electrical and thermal properties

Semicrystalline materials generally have greater dielectric absorption and greater short-term breakdown field than amorphous materials, and these two properties are probably coupled. Dielectric absorption results, in part, from the differing electric field distribution for the capacitively graded and resistively graded conditions. For a perfectly amorphous (homogeneous) material, which does not exist, these two field distributions would be the same, and, in the absence of electrode effects, the material would go into immediate steady state DC conduction. For an inhomogeneous material, e.g., a semicrystalline material, the electrical conductivity is inhomogeneous which results in an inhomogeneous field distribution and space charge formation under DC conditions. This also implies greater electric field in the low conductivity regions than in the high conductivity regions relative to the capacitively graded condition. The change in the field distribution within the

dielectric during the transition from capacitive to resistive grading after application of a voltage results in an external "absorption" current. This current, at low fields, relaxes to a steady state DC "conductive" current over minutes to hours as a result of the dielectric time constant(s), ε/σ, within the material. When a ramp voltage to breakdown is applied, the field becomes sufficiently high to reduce the dielectric time constant within the material from minutes/hours to seconds, so that the relaxation takes place very quickly and gives rise to a measureable current which is the sum of the absorption current and the high field DC conduction current [134,135]. This relaxation also results in redistribution of the electric field with greater field within the higher strength, low conductivity regions and reduced field within the higher conductivity, lower strength regions. These phenomena result in the general trend that breakdown field increases with crystallinity (inhomogeneity), although some amorphous materials have outstanding breakdown field.

Thermal conductivity, especially in-plane thermal conductivity, of capacitor films is very important to their application, as polymers generally have poor thermal conductivity, heat is generated within capacitor windings, and, in the case of metalized film capacitors, such heat must be removed by conduction in the polymer film. The in-plane thermal conductivity of a thin polymer film is also a function of the morphology, as in insulators, heat is carried primarily by phonons, which are creatures of the polymer backbone. In highly oriented polymers, such as almost perfectly linear PE, thermal conductivity in the direction parallel to the polymer backbone can be two orders of magnitude greater than for bulk (random) PE [136]. In the case of BOPP, the average in-plane thermal conductivity is over twice that of bulk PP [137] as a result of the orientation, which takes place during biaxial stretching.

In order to emphasize the importance of thermal behavior, we make the following observation. BOPP presently dominates high energy density applications, and improvements to energy density and/or operating temperature would not be useful if the film in-plane, transverse (to the machine direction) thermal conductivity dropped from the range of 0.7 W/m K (BOPP) to 0.2 W/m K which is typical of amorphous polymers. For example, increased dielectric constant implies reduced winding length for a given film thickness and active width. Decreased winding length increases effective series resistance from the film metallization and decreases the cross section available to remove heat from the center of the winding. Thus, improving and controlling thermal transport (which in turn is controlled by structural morphology) is of paramount importance.

2.4.2. Prediction of the unit cell level of structure of crystallites

While conventional analytical characterization methods are available to examine the structure of polymeric materials at various length scales (ranging from birefringence to assess crystalline content/orientation, wide angle and small angle X-ray diffraction to determine crystal type, atomic force microscopy to assess morphologies at or near the surface of the films [138–140]), determination of the unit cell level crystalline structure of a given polymer is never straight forward. The emerging computational structure prediction approaches provide an alternative to synthesis and characterization. The work of identifying the possible structures of a hypothetical material is mathematically formulated as an optimization problem, locating the low-lying local minima of the potential energy surface (PES), which is usually constructed based on the DFT energy. Finding the global minimum would be ideal, but no method presently exists that is capable of doing so. Fig. 17 illustrates a potential energy surface which contains many local minima distributed over configurational space. Common DFT packages can effectively perform local optimization, i.e., given an initial structure, a "nearby" equilibrium structure (a local minimum of PES) can be located (see Fig. 17). Escaping this local minimum to explore other minima requires a global optimization algorithm that is not presently available. Computational/theoretical schemes designed for finding new material structures (or equivalently, for locating new local minima on the PES) prior to synthesis are typically referred to as *materials structure prediction* methods [141,142]. In the early days, the inability of the structure prediction methods in identifying even the simplest crystal structures was cited as a "continuous scandal in the physical sciences" [143]. The situation has improved in recent years thanks to the development of efficient algorithms and powerful computational capabilities [26,32–34,36,141,142,144–146].

Modern structure predictions algorithms such as USPEX [147], minima-hopping [148,149], CALYPSO [150], and random search [151] are normally coupled with a DFT package to calculate energies and forces/stress, but differ in their algorithm for global optimization. USPEX uses an evolutionary algorithm, CALYPSO uses a particle swarm optimization algorithm, minima-hopping and random searching methods use the algorithms with the same name. At a larger scale, the ant colony optimization algorithm has also been used in a protein folding prediction [152].

Searches for materials structures are usually performed without constraints, that is, all the configurational degrees of freedom of the structure are treated independently. Because the configurational space is astronomically large, this is not the most efficient strategy for organic polymers, whose structures are typically described as a certain packing of linear chains of atoms/functional groups (see Fig. 18, where the structure of PE is shown as a packing of linear chains of CH_2 blocks, for an illustration). The restricted and well known nature of organic compounds implies that certain geometrical constraints can be implemented to downsize the searching space, which results in more efficient prediction of possible structures. In such a constrained polymer structure prediction method [144], the constraints are implemented in a pool of pre-defined blocks, e.g., $-CH_2-$, $-C_6H_4-$, and $-CHCl-$, which are considered building blocks of the polymer structures. For use with the evolutionary search algorithm as implemented in the USPEX code [147,153], a population of symmetric structures of these blocks is generated and allowed to evolve over a number of generations, minimizing the associated DFT energy. This approach is efficient at recovering the correct structures of many polymers [144], e.g., PE, polyacetylene, and poly(glutamic acid), and predicting the structures of newly-developed high dielectric constant polymers discussed in Section 4 [26,34–36,144].

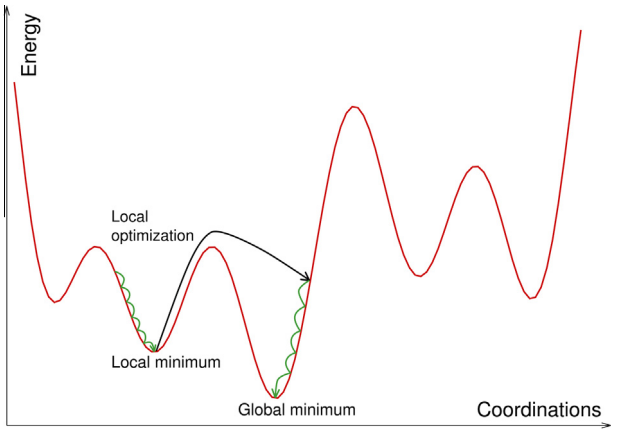

Fig. 17. An illustration of the potential energy surface, given as a function of the system coordinates. These are many local minima of the surface, and the local optimizations performed by a regular DFT code are sketched in dark green. A structure prediction method is typically needed to "escape" the current local minimum (the process sketched in black), exploring new local minima.

Organometallic polymers, also discussed in Section 4, belong to another a major class of energy storage materials in which metal atoms are incorporated directly into the polymeric backbone. Because metal atoms can generally adopt multiple coordination environments, the blocks and constraints are not well defined. In this case, unconstrained search methods can be used. The minima-hoping method [148,149] has revealed unexpected polymeric structure for various families of organometallic polymers, which were subsequently confirmed experimentally [32,33,57].

2.4.3. Prediction of larger scale morphology using MD

While DFT based ground state structure prediction methods are becoming available to address the atomic-level polymer structure, these approaches still have two limitations, viz., (1) practically, they can only treat unit cells of modest size (a few tens of atoms or less), and (2) effects of non-zero temperature are not included.

The melt-and-quench approach adopted widely in force field based MD simulations fills the gap effectively, at least in cases for which reliable force fields are available. In order to address on the power (and the deficiencies) of this approach to structure prediction, we take a specific relevant example. Predicting the morphologies into which vinylic polymers crystallize into is one of the outstanding challenges in the modeling community. Long chains of the simplest vinylic polymer, i.e., polyethylene, crystallize into a single morphology, namely an orthorhombic structure, where the chains assume all trans (or herringbone) conformations. Almost all other stereoregular polymers assume multiple structures, with differing structures as a function of chain length, the temperature, and pressure at which the crystallization process is conducted. Lovinger et al. [154] have reviewed the various crystalline forms of isotactic (iPP) and syndiotactic (sPP) polypropylene. For example, iPP forms in three differing morphologies, the α, β and γ phases, for which the chains always assume a helical conformation. sPP assumes four differing morphologies, with two involving helical conformations and the other two planar all trans states. This problem is very complex, so that *a priori* prediction of the various crystal states that can be formed by a given polymer is difficult.

Over the last few decades, several groups have attempted to use molecular simulations to tackle this difficult, but important problem. Muthukumar and coworkers [155,156] used simulations, both from solution and the melt, to examine the early stages of crystallization, as well as the structure of the crystalline lamellae that form. Gee et al. [157] were one of the first to simulate the crystallization of iPP from the melt using all atom MD simulations. These workers also focused on the time evolution (especially the early time behavior) of the crystallization process. Gautam and coworkers [158] took an alternative approach and looked at the behavior of known crystalline morphologies – that is, they did not attempt to predict crystal morphologies, but rather used molecular simulations to predict the properties that result from known crystal

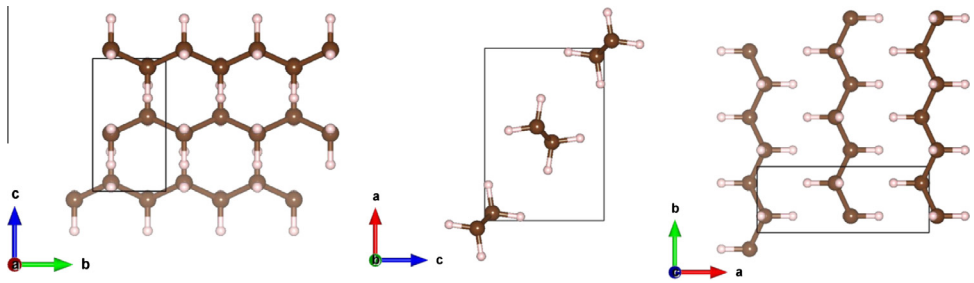

Fig. 18. Views of polyethylene crystal structure along the *x*, *y*, and *z* directions. Carbon and hydrogen atoms are shown in dark brown and pink.

structures assumed by a given polymer. What remains problematic are two trains of thought: (i) we do not know how to predict the various crystal structures into which a polymer crystallizes and (ii) even in the few limited cases where we can simulate the structures, we are limited by the inaccuracies of the force fields involved. Thus current force fields (OPLS for example) will predict that sPP will crystallize into an all trans state under quiescent conditions, while experiments uniformly show that this structure will only occur in the presence of stress. Little progress can be achieved in this area until force fields become sufficiently accurate to predict known experimental results correctly.

2.5. Film formation and rheology

For a potentially useful polymer to be fabricated into a capacitor, a thin film must be manufactured. A capacitor dielectric must have sufficient tensile strength and acceptable rheological properties to be wound as a thin film at high speed without stretching (which is one reason that PE is seldom used as a capacitor dielectric). It also must be sufficiently pliable to be handled without "flaking", "cracking", etc. To obtain optimum mechanical, thermal and electrical properties, the film formation step is important.

2.5.1. Processing to make films

A capacitor dielectric film can be solvent cast or melt processed. Solvent casting is much more expensive, in part as a result of environmental issues. Thus melt processing is much preferred but requires that the polymer melts below its thermal degradation temperature, which becomes an issue for high temperature polymers. For melt processing, a polymer must have rheological properties which allow it to be extruded and then stretched to a thin film, usually by a bubble or tenter process. For both solution processing and for melt processing, a polymer must have sufficiently high molecular weight to offer good rheological and mechanical properties to allow them to be solution cast or melt extruded and then stretched to a thin film.

Solution casting is always complicated by the presence of residual solvent that can affect electrical properties adversely. Melt processing methods include single or double bubble [159] film blowing and tenter frame biaxial film stretching [160]. Coextrusion and microlayer coextrusion [161–164] processes may enhance the mechanical and/or electrical properties of films by creating a multitude of alternating polymer layers that change the mechanical, diffusion, and electrical properties. After extruding a relatively thick film, the tenter stretching process is often adopted to orient the film biaxially [165–167] and cause strain induced crystallization when possible. During a final stage of heat treatment (called heat setting), crystallinity can be increased substantially at the expense of oriented amorphous chains, resulting in a polymer film with high thermal stability [168]. Materials which crystallize rapidly, such as PP, PE, and PVDF, are melt cast and subsequently stretched at temperatures at which their crystalline portions are partially molten.

To achieve uniform deformation during stretching, polymers must have small crystallites after casting so that when reheated and stretched, they exhibit pseudo affine deformation, as the deformation tends to concentrate at interfaces of the spherulites, where the melting temperature tends to be reduced. Occasionally nucleating agents are added to reduce the crystallite sizes for this purpose. The quenched film is reheated to a temperature at which it is partially molten. The optimum temperature is about $\frac{1}{3}$ way between onset of melting and peak melting temperature. In this partially molten state, small lamellae/crystallites melt, and these may be located at the boundaries of the spherulites which facilitates deformation. During the deformation stage, the intact lamellar structures may break into blocks and rotate in the plane of the film, reestablishing a new oriented morphology with oriented crystallization of the previously molten chains. As the last step, the film may be subjected to heat setting during which it is constrained dimensionally while heated to an appropriate temperature to relax some of the oriented and uncrystallized chains, which improves dimensional stability at elevated temperatures. In the case of metalized film capacitors, this last state is often carried out after winding.

Materials with slow crystallization such as PET, PEEK, and PEK typically have relatively stiff chain backbones which results in T_g above the room temperature. Such polymers can be quenched into a glassy state through solution or melt film formation, after which are heated, stretched either uni-axially in the machine direction or bi-axially using tenter frame at a temperature between their T_g and T_{cc} (cold crystallization temperature) over which they exhibit very high viscosities which facilitates substantial orientation of polymer chains resulting in strain induced crystallization. Films processed in this manner tend to have high concentration of oriented amorphous chains. Unless they are stabilized thermally in a final heat setting stage of the tenter frame process, this would lead to shrinkage related distortions. Hence they almost always are exposed to a temperature typically halfway between T_{cc} and melting temperature that causes rapidly crystallization of the oriented amorphous chains and facilitates relaxation which results in much more dimensionally stable film. Such relaxation also enhances the material's dielectric properties significantly, as the crystallinity increases to 40–50% from the original as-stretched state of 25%.

2.5.2. Rheological properties

Rheological properties are related to the molecular architecture of the polymers to be processed. Molecular weight (MW) must be sufficiently high to obtain good solution and melt properties that facilitate film formation and subsequent stretching operations. Too low a MW causes embrittlement in many cases. Polymers rheological properties are modified for each process. For example, polypropylene resin used in the bubble process of film formation differs subtly from that used in

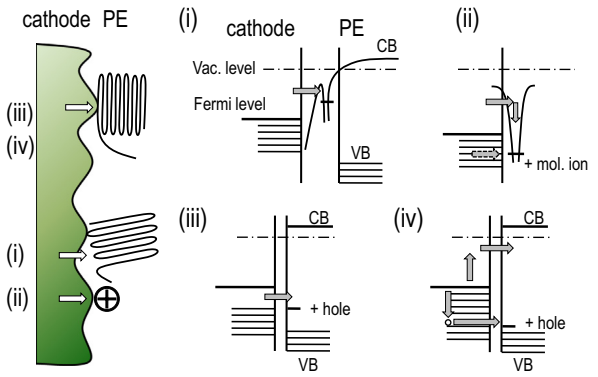

Fig. 19. Various processes for electron transfer at cathode–PE contact. (i) Emission into quasi-vacuum state. (ii) Positive ion and (iii) positive hole neutralization. (iv) Electron tunneling to hole in polymer chain creating hole in metal. Subsequent downward Auger electron transition to hole releases energy. Figure reproduced following Ref. [133].

the tenter process. Typically, broad molecular weight PP is used for tenter frame and blown film operations with reduced crystallinity in the latter. The resins marketed for this purpose are very "clean".

For microlayer coextrusion, the rheological requirements are quite stringent as the two materials that are brought together in stacked form in-molten state and are repeatedly split lengthwise, restacked and squeezed as they go through flow multipliers to geometrically increase the number of layers to 2^n (with n being the number of multipliers). In this process, the matching of rheological properties of the two materials is critical, and excess melt elasticity would lead to the formation of secondary flows that tend to destroy the uniform layer structure. Thus the resin molecular architecture must be adjusted carefully for this process to work efficiently.

2.6. Metal–polymer interfaces

One of the least studied aspects within the context of polymeric capacitor dielectrics is the role of the electrode/polymer interface. This is rather surprising as charge injection processes originate at this interface. Uncontrolled and persistent interfacial charge injection (especially under AC field), determined by the charge injection barriers (CIB) at the interface, can lead to progressive degradation, and ultimately, to the failure of the embedded polymer dielectric layers [169]. The CIB at a metal–dielectric interface is, in principle, determined by the appropriate electronic properties of the metal (i.e., its work function), the dielectric (i.e., its band gap and electron affinity), and the interfacial region (i.e., its dipole moment, Fermi level pinning) [43]. However, the real situation is much more complex.

2.6.1. Experimental characterization of metal/polymer interfaces

Although organic polymers are simple at an atomic level (mainly composed of small atoms such as C, H, and O), they are complex at the morphological level due to presence of various amounts of crystalline and amorphous regions. As a result, the interface between a polymer and metal is complex, as the metal interfaces with both the amorphous and, if present, crystalline regions of the polymer. In addition, the polymer surface to which the electrode interfaces typically differs from the bulk. Thus in the case of semi-crystalline polymers, electrode contact can never be uniform on the scale of the polymer morphology. The contact area consists of electrode interfaces to lamellae of various orientations, to individual polymer chains in amorphous regions and to voids and impurity molecules [133,170]. This situation produces various mechanisms for electron transfer from the cathode to the material as shown in Fig. 19.

Polymer dielectrics also contain chemical defects, e.g., occasional CO (or carbonyl) groups instead of CH_2 units in PE [102]. In the most experiments, the electrode is metal covered with oxide or other contact impurities. All these aspects affect the electronic structure across the metal/polymer interface. Unraveling the specific roles of the various relevant factors in determining the CIB is far from trivial. This complex situation is well illustrated by the discrepancies between experimental measurements and theoretical prediction based on simple electronic properties. For example, the current measured in metal–insulator–metal (MIM) structures is several orders of magnitude greater than that predicted by the Schottky equation when using the theoretical barrier height expected for a metal/polymer contact, and stored charge quantities do not vary in the expected way as a function of the metal work function [171–173]. These discrepancies are generally understood in terms of surface states (and, more generally, in terms of interfacial states), that result from such physical/chemical complexity. Whatever their origin, surface states correspond to localized energy levels in the band gap. The surface states promote charge injection from the metal to the dielectric by creating localized states that assist tunneling through the barrier [174,175,170].

The process by which the interface is created can affect the metal/polymer interface, e.g., thermal evaporation of metal for metalized film capacitors or extrusion of a carbon black filled semiconducting layer for solid insulation cable. Each process affects the polymer/electrode interface in a specific way, such as penetration of metal atoms into the polymer film during thermal evaporation in metallized film capacitors and diffusion of ionic species from the semi-con layer into the insulation

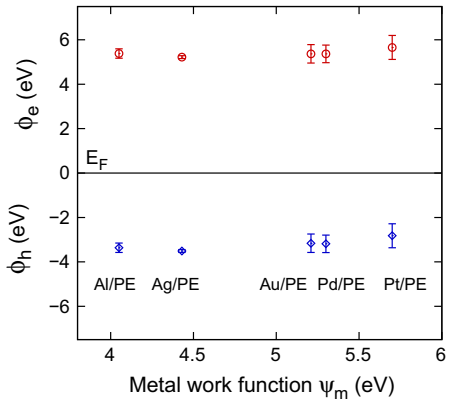

Fig. 20. Charge (electron and hole) injection barriers calculated for the interface between polyethylene and different metals. The error bars represent the spread of the computed barrier heights for a few different choices of the atomic-level structure of the metal–PE interfaces. Figure adapted from data reported in Ref. [43].

in cables [128]. Note that in the latter case, a thick solid dielectric layer bounded by semiconducting layers on both sides is often extruded in a single step process, and cooling of the structure is inhomogeneous, which results in a gradient in the microstructure of the polymers and, often, a specific orientation of the molecules at the interface [176]. In addition, the interfacial region changes from some tens of nm in semiconductors [177] to μm in capacitor films and 10s of μm in cable dielectrics [170]. Such large differences in the extent of the interfacial region are related to the nature of "defects" at the interface. Metal-induced defects in crystalline materials should be restricted to the crystal surface. When surface states are related to residues or oxidation, as in the case of polymeric insulating materials, the interfacial region is much greater. Experimental and theoretical data for charge injection at a PE/metal structure have been reconciled by assuming a gradient in the density of states within the band gap as a function of the distance from the electrode [172].

2.6.2. Computational characterization of metal–polymer interfaces

Determining the CIB for *realistic* metal/polymer interfaces using density functional theory (DFT) is in its infancy, although the theory for determination of the CIB, given the interfacial atomic-level structure, is available. For cases where the interface structure is much less complex than in metal/polymer interfaces (such as GaAs/AlAs [178], SiO_2/Si [179], HfO_2/Si [180], and HfO_2/metal [181–183]), the CIB and the effective work function (a related quantity) have been computed with acceptable accuracy. The parameters necessary to compute the CIB for a metal/insulator system include the work function of the metal, ψ, the band gap, E_g, and the electron affinity, E_{ea}, of the insulator, and the interfacial dipole moment-induced vacuum level shift $\Delta\phi$. Except for the last quantity ($\Delta\phi$), the required properties relate to the interface. The dipole moment is related to the interfacial structure and bonding. A lack of knowledge (or an incorrect assumption) of the nature of the interface will lead to errors in the prediction of the dipole moment, and hence the CIB.

In recent work [43], the CIB of metal–PE interfaces has been computed using DFT, for Al, Ag, Au, Pd, or Pt, which are conventional choices for practical and model electrodes. Three contact geometries between PE and the metal were considered in an attempt to span a few extreme cases of interface configurations. Fig. 20 shows the electron and hole CIBs for the five metal electrodes. Each of the computed quantities, namely, the metal work function, the PE band gap and electron affinity, and the dipole moment induced at the metal–PE interface, compare well with available experimental data. Trends in the computed CIB values for electrons and holes, and the (lack of) variation of the CIB with the choice of the metal are also in favorable agreement with measurements [184,185]. Nevertheless, discrepancies remain with respect to quantitative correspondence between the computed and measured CIB values. These can be addressed adequately only if more realistic models of the metal/PE interface (including morphological complexity and chemical defects) are included in the computations. Such information can come either from MD simulations of the interface, or from physical and electrical characterization of metal–polymer interfaces in the future.

2.7. Capacitor performance

2.7.1. Capacitor

The electrical properties of a capacitor are a function of both the materials the capacitor is composed of (dielectric, metallization, etc.) and the structure (film width, enclosure, etc.). A capacitor can be characterized by its equivalent series resistance caused by metallization resistivity, which is independent of frequency, its dielectric loss, which is often frequency-dependent, leakage resistance as a function of temperature, resonant frequency (or equivalent series inductance), etc. Dielectric loss in a metalized film capacitor is dominated by two phenomena that differ greatly, viz., I^2R losses in the resistivity of the metallization and dielectric loss in the capacitor film. End connection losses are usually negligible [186]. I^2R losses depend only on the RMS current and are independent of frequency, as the film metallization forms a nearly ideal

resistor. Dielectric losses depend on relaxation phenomena in the film and, at high temperature, on conduction through the film. As a result, dielectric loss is a function of both frequency and temperature, especially for polar dielectrics, and characterization is better carried out on film sample rather than on a capacitor winding. Since the two major sources of loss are the result of differing phenomena, they should be characterized separately and reported separately. The I^2R loss is a function of the metallization and extrinsic to the film, while the dielectric loss in the film is a material property thereof and difficult to change. For very low loss films such as BOPP and PS, metalized film capacitor loss is dominated by the metallization resistivity. For higher loss materials such as PET and PVDF, the dielectric loss of the film makes a significant and often dominant contribution to the total loss of the capacitor.

From a practical perspective, a total loss below 10^{-3}, the typical loss of a metalized BOPP film capacitor, is negligible for most purposes. A dielectric loss of 10^{-2} approaches the upper limit of a useful capacitor and limits application to low repetition rate pulse discharge, low ripple voltage DC link, etc., i.e., to applications where the capacitor has time to cool between discharges or to applications where the ripple voltage across the capacitor can be limited, as in DC link applications.

Capacitor loss, inductance, and thermal properties depend strongly on capacitor structure, in particular the film width selected to wind the capacitor, the manner in which the capacitor terminals are connected to the winding, anisotropic thermal conductivity of the film, thermal coupling between the film of the winding and the case, etc. A capacitor is a complex device that is difficult to characterize fully. Viewed as a 2-terminal electronic component, it is often characterized by an equivalent series resistance, an equivalent series inductance, and a temperature rise constant between the peak temperature in the capacitor and the power dissipated therein. Depending on the application, the capacitor may also be characterized for maximum current as a function of ambient temperature, peak discharge current, etc. A global ESR, which does not separate contributions from metallization and film dielectric loss, is typically frequency-dependent for polar dielectrics.

The connections to metalized film (end connections) are effected through an axial offset of the two metalized films by a few mm, with the projecting edges metalized to the edge while the opposite film edges have an unmetalized margin of several mm. Each end is wire arc sprayed with metal, usually Zn or a Zn alloy, to connect to the metallization of the film. Since the edge of the film is not metalized (as the film is slit after metallization), the metal spray particles must penetrate between the film layers to make connection to the evaporated Al film metallization. The Zn particles, even if molten, will not bond metallurgically with the Al metallization. In the case of BOPP, the film shrinks above about 110 °C, so that the film shrinks around the hot metal spray particles, which provides a degree of adhesion. Typically, the spray particles do not penetrate uniformly, so that connection between the spray and the film metallization is somewhat sporadic along the film edge, which can result in excessive current density around some connection points (Fig. 21) [186].

2.7.2. Energy density

Capacitor energy density (J/cm^3 or J/kg) is the holy grail for many pulsed power applications, but charge–discharge efficiency is equally important because high energy density is usually achieved by charging to very high field, at which conduction, polarization, etc., become appreciable and reduce the fraction of energy that can be recovered during a discharge. In steady state, that difference must appear as heat in the capacitor, and in very large capacitors, the operating time at a given rate of charge–discharge is limited by the energy dissipated in the capacitor per discharge and the thermal time constant of the capacitor, which is typically dominated by heat capacity. The standard laboratory approaches for measuring loss

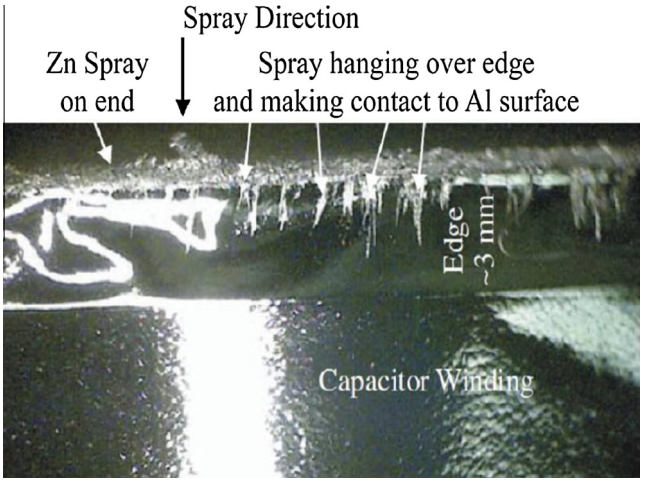

Fig. 21. Photomicrograph of an end connection during unwinding of a capacitor winding. The view is radial near one end of the winding. The heavily metalized region of the metalized film is near the top. The softness apparent in the upper 3 mm of film is the result of the film offset, which leaves the protruding film essentially unsupported. The wire arc metal spray is liquid when it reaches the gaps between film layers and splashes into the gap, leaving intermittent filaments of spray metal penetrating along the surface of the metalized film. The connection is sporadic and tenuous, the implications of which for electrothermal failure of the end connection have been explored in Ref. [186].

(dielectric spectroscopy, D-E loops, etc.) are of very limited use for predicting the performance of a large capacitor during a charge–discharge cycle, and laboratory characterization requires specialized high power apparatus. On the other hand, the performance in a large capacitor is unlikely to be better than that determined during laboratory characterization of the film, but it can easily be much worse. Thus laboratory characterization using, for example, a D-E loop, is sufficient to eliminate a material but it is not sufficient to assure that it will perform adequately in a large pulse discharge capacitor.

3. Recently considered materials

The previous section discussed a hierarchy, or constellation, of properties (ranging from dielectric, electronic, chemical, structural, processing, and electrical aspects) important in determining whether a given material will be suitable for high energy density capacitor applications. *As must be evident, the road to the success of a particular material is punctuated with an enormous number of barriers and challenges*. A successful capacitor film must meet a wide range of requirements, which makes discovery of appropriate materials problematic, as does our inability to predict all of the relevant properties. We noted in Section 1 and Table 1 that the polymer dielectrics that have dominated high energy density applications in the past several decades are BOPP, PET, PC, PPS, etc. In recent years, a range of seemingly promising material systems have been investigated based on search strategies ranging from Edisonian approaches, intuition, and computations. The community is gradually moving from empiricism to more computationally directed concepts. In this section, we provide a survey of such recently considered and emerging materials.

3.1. PVDF and variants

The history of PVDF film-based capacitors is well over 30 years old. For example, a 1981 paper [187] discusses the properties of both metalized film and film-foil capacitors based on PVDF film. In 1993, General Atomics manufactured a 16 kV, 125 kJ capacitor based on biaxially oriented PVDF (BOPVDF) film with an energy density of 2.4 J/cc [188]. The attraction of such film includes a dielectric constant in the range of 11 and a breakdown field comparable to BOPP. The limitations of capacitors made with biaxially oriented PVDF film include relatively high loss ($\sim$1%) and a discharge energy density that decreases for discharge times below the millisecond range. The latter may contribute to the very high breakdown field of biaxially oriented PVDF. This combination of properties limits the application of biaxially oriented PVDF-film based capacitors to ms discharge, low repetition rate applications such as aircraft carrier catapults. The detailed dielectric properties of biaxially oriented PVDF and prospects for its use as a practical capacitor film were recently examined in Ref. [5].

Starting around 2000 [6], attempts began to retain the advantages of PVDF and overcome some of its disadvantages through development of ferroelectric relaxors based on copolymers, terpolymers, etc., with the intention of reducing the cooperation on which ferrorelectric behavior depends through defect-induced pinning, reduced interaction between dipoles as a result of reduced dipole density, and/or reduced domain size [7–9]. While some of the resulting polymers nearly eliminated hysteresis in the D-E loop at the expense of greatly reduced dielectric constant [10], none retained sufficient advantages of substantially increased dielectric constant with sufficiently low loss ($\ll$1%) or improved charge–discharge efficiency to form the basis for a practical capacitor dielectric [10,11]. Thus, despite the exciting scientific prospects, this approach to improved capacitor dielectrics appears to have slowed down due to practical challenges.

3.2. Multilayers

The technology for manufacturing multilayer films has existed for many decades; however, the manufacture of such films as high voltage dielectrics is quite recent. Conventional "laminar" dielectrics, i.e., those formed from multiple, independent layers, have the advantage that defects in adjacent layers are uncorrelated, as a result of which breakdown voltage for such dielectrics increases more or less in proportion to the number of layers, while the breakdown voltage of a bulk dielectric increases more or less as the square root of its thickness as defect "size" is not limited by layer thickness. Coextruded multilayer dielectrics fall somewhere between these two extremes as (i) the multiple "folds" necessary to form large numbers of layers may trap contaminants between "folds" which can protrude into adjacent layers, and (ii) the very large interfacial area invites defects.

Much of the published literature on multilayer dielectrics has been devoted to phenomena such as inhomogeneous field breakdown, which has been used to investigate the effect of "tree-like" breakdown patterns on layer adhesion and interfaces [12,13]. Such studies follow from the fact that the materials from which multilayer films are made must "stick" to each other to avoid delamination, but at the same time they must be immiscible, a combination which invites studies related to the degree of adhesion between layers and the effect thereof on dielectric performance. However interesting these phenomena may be at a fundamental level, they have little relevance to highly uniform field conditions within a capacitor, for which breakdown is normally a single step process.

Data and analysis closely related to uniform field laminar dielectric applications can be found in [15,16]. In Ref. [15], the authors provide a Weibull plot of breakdown data for 30% polysulfone, 70% poly(vinylidene fluoride) films of varying numbers of layers and thickness. The Weibull characteristic breakdown field ranges from about 313 to 416 MV/m with the Weibull slope parameters which vary from 6 to 13; however, given the relatively small numbers of breakdowns per sample

(about 20), the variation in the Weibull slope parameter may not be significant. The greatest Weibull characteristic breakdown field results from a 11.6 mm, 32 layer sample, while the lowest results from a 256 layer, 12 μm thick sample. The authors investigate this difference based on "aging" studies and conductivity measurements.

Ref. [16] is an excellent study of the dielectric loss observed in 50% polycarbonate, 50% PVDF films of varying numbers of layers (layer thickness). The authors demonstrate that the loss is not caused by a ferroelectric effect in the PVDF component and demonstrate that the loss is caused by ionic mobility in the PVDF component, as loss reduces with decreasing PVDF layer thickness because ions are immobilized by the layer interface earlier in the AC cycle with decreasing layer thickness.

Concerns related to multilayer dielectric technology for application to capacitors center on manufacturing cost (line speed) and dielectric performance. To date, no data have been published which demonstrate significant improvement in performance over single layer dielectrics for applications to metalized film capacitors.

3.3. Nanocomposites

The concept of filling a polymer with high dielectric constant microscopic particles or nanoparticles, often referred to as fillers, also has a long history [17–22,24,25]. This approach, which is rationally motivated by the "mixing rules", relies on combining high dielectric constant fillers in a high breakdown strength polymer [20,22]. The fillers can either be inorganic, e.g., metals, ceramics, and carbon-based materials, or organic, e.g., semiconductive olligomer and conducting polymers [20–22]. In ceramic–polymer composites that utilize traditional ceramics like $BaTiO_3$, $BaSrTiO_3$, and $PbZrTiO_3$ as fillers, an issue arises due to the deterioration of the mechanical properties due to the highly-concentrated presence of rigid ceramic particles [20]. If conductive nanoparticles (silver flakes or Ni) are used as fillers, the dielectric constant can be boosted up to hundreds or thousands [23,24] at the price of remarkable increase in electrical conductivity, the dielectric loss, and the sensitivity of the dielectric constant to the concentration of the fillers [20]. Different from these filler options, nanotubes with superior electrical properties can offer better mechanical properties [189] and larger surface area, which ultimately lead to better dielectric properties [190,191]. However, primary concerns pertaining to the processing aspect have not been solved yet [20]. In spite of different strategies employed, the agglomeration of the nanotubes and their incompatibility with the host polymers remain challenging [20]. Semiconducting and conducting organic filers are also interesting as these types of fillers can improve the dielectric properties of the host polymers without seriously deteriorating their mechanical properties [192].

Another theoretical consideration that supports the nanofiller approach is the possibility of controlling filler–polymer interfacial polarization and the electric field distribution [22]. The enormous interfacial area (especially in nanocomposites) potentially creates new, highly polarizable extended phases in the interfacial region that can enhance the dielectric constant of the filler particles and modify the electric field distribution in their vicinity. Key to this approach is the need for intimate chemical bonding between a polymer and the filler particle surfaces [22]. Recent chemical ingenuity has made such coherent interfaces possible [17]. Challenges with this approach remain. Below percolation of the high dielectric constant filler, most of the electric field is in the matrix and the filler acts similar to a "conductor" in that it nearly excludes field from within it and, as a result, enhances the field in the matrix, thereby reducing the breakdown field of the composite (although this effect is reduced through the use of nanoparticles) [17–19]. As the volume fraction of the filler approaches percolation thereof, the field in the filler increases rapidly, which results in a consequent increase in the composite dielectric constant with filler concentration. Percolation for spherical particles is in the range of 35% volume fraction. Graded dielectric constant nanofillers have been used in an attempt to overcome the above issues, but the efficacy of such an approach is not yet clear.

3.4. Functionalized polyolefins

Recent experiments demonstrate 4–6 mol.% hydroxyl (–OH) side groups added to PP nearly doubles the dielectric constant with minimal impact on the semicrystalline morphology [193]. This finding is significant as it provides a pathway to increase the dielectric constant of PP [194–196]. Detailed infrared characterization and dielectric spectroscopy studies at various temperatures provide compelling evidence for the role played by the –OH groups, leading to the conclusion that these species exist in the amorphous parts of the polymer in a hydrogen-bonded state. The presence of water molecules in the hydrogen-bonded regions was also surmised. Subsequent analysis of this system by MD simulations coupled with DFT calculations further affirmed that hydrogen bonds between water and adjacent –OH groups result in this higher dielectric constant without a major increase in dielectric loss [197,198]. A central assumption of this past is that the morphology considered in the simulations is not critical to the prediction of the dielectric constant. This conclusion follows since the MD results (which deal with a semicrystalline morphology, with both crystalline and amorphous components) are in good (qualitative) agreement with the DFT results, which only deals with the crystalline component.

More recently, the focus shifted to examining the dielectric constant of PE chains functionalized with a fixed concentration (4.2 mol%) of various polar groups. A series of DFT and MD simulations were carried out based on functionalizations of $–CH_3$, $–NH_2$, $–NO_2$, –COOH, –OH and –SH. Two flavors of MD simulations were performed: one on the ground state crystal structure simulated by DFT and a second self-assembled semicrystalline state formed spontaneously by these polymers when cooled from the melt to a temperature below their equilibrium melting points. The dielectric constants found in the first set of simulations are in quantitative agreement with the DFT calculations for the polar component of the dielectric constant. This close agreement validates both the MD and the DFT protocols. However, the MD simulations using a semicrystalline state yields ionic contributions to the dielectric constants that are up to 10 times larger than those obtained from the

DFT crystal simulations. An equilibrium statistical thermodynamic argument suggests that this reduced dielectric constant in the DFT calculations is a direct consequence of significantly reduced dipole moment fluctuations in the crystalline state relative to the amorphous state. These results therefore emphasize the important role of polymer morphology in predicting the dielectric constant of functionalized polymers. More broadly, the approach of funtionalizing PP with polar groups appears to be a promising direction worthy of further enquiry both on the experimental and computational sides.

4. Emerging materials platforms and search paradigms

More recent efforts have taken a fresh look at the truly staggering polymer chemical space defined by the basic polymer building blocks [26–28]. One of the advantages of utilizing computations is that initial screening can be carried out in a cost-effective and efficient manner. Promising new organic polymers were identified based on their dielectric constant and band gap, both of which can be computed with reasonable accuracy using quantum mechanical computations [26–28], and then synthesized and characterized experimentally. As must be apparent from the discussion in Section 2, dielectrics for high energy density capacitor applications need to satisfy additional requirements, including low dielectric loss, high dielectric breakdown strength, etc., thus making the adopted screening criteria necessary but not sufficient conditions. Nevertheless, these recent attempts, although based on limited initial screening criteria, have provided promising candidates worthy of in-depth investigation. Furthermore, computations involving a class of synthesized polymers containing metal atoms have also helped unravel and understand the structural details of the synthesized polymers. This aspect is just as important to timely success as pointing toward the "right" polymers in the first place. We now briefly describe these emerging rational dielectric discovery paradigm.

4.1. New organic polymers

We first consider organic polymers. The screening step started from the following pool of building blocks, which are common in polymer backbones: $-CH_2-$, $-C_6H_4-$, $-C_4H_2S-$, $-NH-$, $-CO-$, $-CS-$, $-O-$. A given number (four in this case) of these blocks were selected to construct the repeat unit of a hypothetical polymer. After the elimination of obviously unstable combinations of these building blocks (such as systems containing contiguous –CO– or –O– blocks) and accounting for translational and inversion symmetry, a few hundred unique repeat units were identified [26,27]. For each, a 1D chain of identical repeat units was built. DFT calculations determined the optimal 1D structure and estimated the band gap E_g and the dielectric constants ϵ_{elec}, ϵ_{ionic}, and $\epsilon = \epsilon_{elec} + \epsilon_{ionic}$. Fig. 22 shows the relationship between ϵ_{elec}, ϵ_{ionic}, and ϵ vs. E_g calculated for the wide range of polymer chains. Fig. 22(a) shows that the upper bound of the ϵ_{elec} vs. E_g is inversely proportional to band gap, enforcing a theoretical limit on the achievable ϵ_{elec}. On the other hand, ϵ_{ionic}, determined by the infrared (IR)-active zone center phonon modes (that is, the modes that display a time-varying dipole moment) [31], is not correlated with E_g, as seen from Fig. 22(b). Thus ϵ_{ionic} can be exploited to increase the total dielectric constant without compromising E_g [26,27]. Fig. 22(c) shows the variation of the total dielectric constant vs. band gap, which is a 'map' of achievable combinations of these properties within the chemical space explored.

Down selection, starting from this set of polymers with 4-block repeat units, proceeded by considering the polymers with $\varepsilon \geqslant 4$ and $E_g \geqslant 3$. Polymers that survived this initial screening are predominantly composed of at least one of the polar units –NH–, –CO– and –O– (which tend to enhance the ionic part of the dielectric constant), and at least one of the aromatic rings $-C_6H_4-$ and $-C_6H_2S-$ (which boost the electronic dielectric constant). In a more time-intensive step, the 3D structure, morphology, the dielectric constant and the band gap were predicted for the 1D systems identified in the previous step; these are listed in Table 3. The first three polymers shown in Table 3 were synthesized and tested. The measured properties (structural, electronic and electrical) were consistent with the predictions for all the selected cases. Interestingly, none of these specific polymers has been considered in the past for dielectric applications, although some organic polymers (e.g., polythiourea) within this general class have been developed recently [199], via experiment-driven approaches, and shows promise.

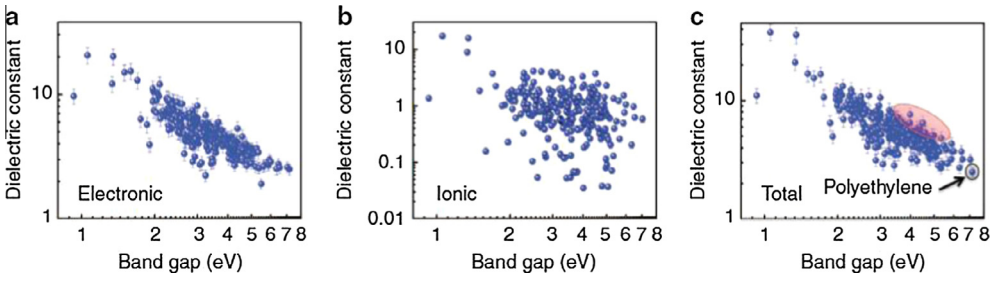

Fig. 22. Computed (a) electronic, (b) ionic and (c) total dielectric constant as a function of the band gap. The highlighted region corresponds to the most 'promising repeat units' composed of at least one of –NH–, –CO– and –O–, and at least one of $-C_6H_4-$ and $-C_6H_2S-$ blocks. Figure taken from Ref. [26] with permission from Nature Publishing Group.

Table 3
Polymers developed by the computation-driven strategy. The dielectric constant and band gap (eV) value ranges shown cover both the computed and measured results, while the breakdown field is a measured quantity.

Polymer	Repeat unit	ϵ	E_g (eV)	E_{bd} (MV/m)	Ref.
Polyurea	–NH–CO–NH–C_6H_4–	5.2–5.7	3.5–4.0	–	[26]
Polyimide	–CO–NH–CO–C_6H_4–	4.3–4.5	4.0–4.1	–	[26]
Polythiourea	–NH–CS–NH–C_6H_4–	5.3–6.0	2.9–3.0	–	[26]
PDTC-HDA	–NH–CS–NH–C_6H_4–NH–CS–NH–$(CH_2)_6$–	3.7	3.5	700	[36]

None of the top 3 synthesized and tested polymers of Table 3 was amenable to film processing however. Ingenious synthetic chemistry was necessary to make one of the candidates processable, based on a variation of one of the original recommendations: [–NH–CS–NH–C_6H_4–NH–CS–NH–$(CH_2)_6$–], the last entry in Table 3. This polymer has been synthesized, processed into films, and has been tested in detail [36]. Its dielectric constant is over 4 (double that of BOPP), its dielectric loss is low, and its breakdown strength is about 700 MV/m (equivalent to that of BOPP). This strategy based on the combination of computation and experiment [26] has pointed the way to dozens of new, processable polymer dielectrics. A full description of these new polymers can be found in Refs. [26,34–36]. These developments that close the "computation-synthesis-characterization loop" are exciting, and provide hope for rational computationally driven approaches for accelerated materials discovery.

4.2. New organometallic polymers

An altogether new pathway toward advanced polymer dielectrics, also recently explored [32,33,57], involves metal atoms in the polymeric backbone to improve dielectric permittivity. The rationale for this pathway arises from the following considerations. First, depending on the metal included, the metal-containing chemical bonds (such as metal–carbon and metal–oxygen bonds) can be highly polar. Second, the vibrational (stretching and wagging) modes involving these bonds are generally soft, thereby boosting the low-frequency region of the phonon spectrum. According to Eq. (1), this improves the ionic contribution to the dielectric constant at the low-frequency limit.

Screening for promising metal-containing polymers started from the 1D-chain approach previously demonstrated for organic polymers [200–202]. The monomer blocks include group-14 halides like SiF_2, $SiCl_2$, GeF_2, $GeCl_2$, SnF_2, and $SnCl_2$, as well as blocks involving ordinary organic groups such as CH_2 [200]. While ϵ_{elec} of these systems is subjected to the same theoretical limit as discussed in Section 4.1, ϵ_{ionic} of 30 is possible, accompanied with respectable E_g. This interesting finding was the starting point for the subsequent development of a family of organotin polymers.

Polymers containing the Sn-ester block –COO–$Sn(CH_3)_2$–COO– were amenable to synthesis. Fig. 23 shows such a representative polymer formed by the –COO–Sn–$(CH_3)_2$–COO–$(CH_2)_n$– repeat unit. DFT-based structure prediction on several such polymers containing varying numbers of CH_2 units revealed a rich variety of energetically-competing structures in which the polymeric chains can either remain isolated or link together in various ways [32,33]. Further calculations show that these structures feature high dielectric constants (from 4 to 8) and high band gap ($\geqslant$4.5 eV). A series of organotin polyesters were synthesized, characterized, and tested [32,33] with favorable agreement between the measured and computed results. In addition, the measured dielectric loss of these polymers was small (around 1%) while the dielectric breakdown field is ~300 MV/m, resulting in an energy density of roughly 4 J/cm^3 [32,33].

While the final performance of these polymers (measured in terms of the energy density) does not (yet) surpass BOPP, this work shows that an entirely new part of the polymer chemical space involving metal atoms is worthy of further exploration. At this time, tin is not the only good metal for this purpose. Ge-based polymers look promising, but Ge is too expensive to be practical. Thus considerable efforts should be devoted in the future to examine other metals incorporated in an organic framework/backbone.

The above examples are illustrative of the sway and influence first principles DFT-based modeling methods are expected to have in the future rational design of materials in general. Not only do such methods complement empirical approaches by guiding synthetic efforts in terms of specific chemical subspaces to focus on for a particular application, they also help reveal the fundamental reasons a particular subclass of materials is worth pursuing. These notions, within the context of dielectrics discovery, are discussed in detail elsewhere [28].

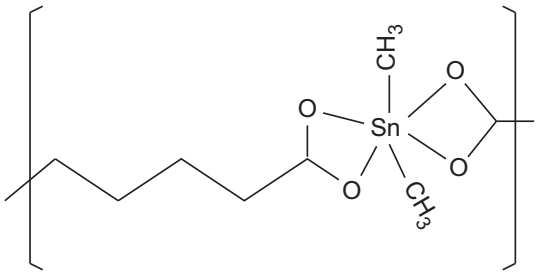

Fig. 23. The tentative repeat unit of poly(dimethyltin glutarate), an organotin polyester with a tin-containing groups linked by three CH_2 units.

4.3. The role of data-driven methods

We end this discussion with the increasing role played by data-driven methods in recent years within the context of materials discovery [52–56]. Data-driven methods have impacted areas such as computer chess, game shows such as Jeopardy, facial and pattern recognition, but are largely untapped within the chemical and materials sciences (there has been recent progress though [52,55,56,54]. The basic premise underlying this paradigm is the following. If we can define a "property space" for a particular problem (in our case, this will be the material properties for each material in the dataset), and a "feature space" (which could be the numerical representation of each material), then a mapping can be established between the two spaces, provided the feature space is complete, relevant and non-redundant. The original dataset may have been obtained by laborious means (e.g., computations or experiments) [203], but once the mapping between the feature and property spaces is established using best-practice statistical methods, the property of a future instance of a new, but similar, situation (i.e., material, in our case) can be computed efficiently using data-mining algorithms instead of explicit (laborious) science-driven computations or experiments. This concept is at the heart of modern data-driven paradigms.

Within the context of polymer dielectrics discovery, the community has amassed an enormous amount of data for a variety of materials (including those that are promising, and those that are not). All this data can be put to use going forward in an attempt to make optimal choices among a myriad of possibilities, and informed "go/no go" decisions on whether new material should be synthesized and tested. This outlook, which incidentally is consistent with the charter of the Materials Genome Initiative [204,205], may well constitute an emerging important component of paradigms aimed at rational, integrated and accelerated materials discovery. However, data-driven schemes are inherently interpolative, making the discovery of truly remarkable "outlier" materials using such techniques a challenge. Still, the effort required in traversing vast chemical spaces will be alleviated by such methods.

5. Concluding thoughts

This review has focused on the progress achieved within the context of polymer dielectric materials development for high energy density capacitors. As highlighted in Fig. 3, several hierarchical considerations ranging from dielectric, electronic, morphological, processing, reliability and electrical characteristics are relevant for the class of applications that rely on high energy density capacitors. The road to the successful identification and optimization of suitable materials is punctuated by enormous fundamental and practical engineering challenges which must be addressed in moving from "standard" materials (such as BOPP) toward next generation materials. While the initial steps in this process, namely that dealing with the dielectric constant, and identification and characterization of pre-existing defects may be viewed as largely "solved" problems (at least computationally), several other enormously important factors such as the dielectric loss, thermal behavior, progressive creation of defects in the presence of a persistent large electric field, and dielectric breakdown are largely "unsolved" problems. The hope for continued progress and ingenuity in this field will be determined largely by new methodology developments to address these unsolved problems based on advanced characterization and materials modeling efforts, and the willingness of the community to tackle the aforementioned problems through synergy between fundamental and engineering efforts.

On the experimental side, advanced in-situ diagnostic tools that monitor pre-breakdown phenomena reliably, such as the progressive creation of chemical defects and changes in structural morphology caused by a persistent and possibly time-varying electric field are essential. Methods to examine and control morphology (e.g., crystallite orientation, crystalline density, surface roughness, electrode–polymer interfaces), and to measure and control thermal transport will be essential. Advanced synthetic methods to handle novel dielectrics and new chemical spaces (e.g., those that involve metal atoms in the polymer backbone with carefully controlled coordination environment to optimize dielectric response) need to come on-line.

The discussion provided in this review also highlights the increasing importance of materials modeling as an essential part of materials development. Several gaps exist as a result of the inability to compute a variety of relevant properties, and with the inability of any combination of presently available methods to treat certain phenomena. Examples of the former include the difficulty of handling morphological complexity and large unit cells with DFT (which is otherwise accurate and versatile), and the lack of universal, accurate and transferrable empirical force fields (which can span larger length and time scales than DFT) to provide acceptable results for a variety of systems of interest. Examples of the latter issue include the inability of any method to predict the engineering dielectric breakdown field of insulators (although DFT can handle intrinsic breakdown), and the difficulty to compute dielectric loss at kHz frequencies (as this will require MD simulations to access ms time scales). Data-driven methods, while powerful, require sufficiently large datasets to produce reliable predictions.

The prospects for systematic approaches toward polymer dielectrics discovery appear to be strong, especially given recent successes and evidence that a cooperative computation-synthesis-processing-characterization paradigm can bear fruit. This approach allows us to go beyond the traditional (but valuable) trial-and-error (Edisonian) and intuition-driven (beyond-Edisonian) approaches adopted to date.

Acknowledgments

RR, SB, MC, and SK acknowledge financial support for their high energy density capacitor materials research from the Office of Naval Research (ONR), most recently through a multi-disciplinary university research initiative (MURI) grant. Several useful discussions with Michele Anderson, Paul Armistead, and Kenny Lipkowitz are gratefully acknowledged.

References

[1] Pollak C. Flüssigkeits-Kondensator mit Aluminium-Elektroden. DRP patent 92564; 1896.
[2] Mansbridge GF. British patent 19451; 1900.
[3] Fitzgerald DG. Improvements in electrical condensers or accumulators. British patent 3466/1876; 1876.
[4] Eckel A. Elektrolytischer Kondensator mit aufgerollten Metallbändern als Belegungen. Deutsches Reichspatent 498794; 1927.
[5] Yang L, Ho J, Allahyarov E, Mu R, Zhu L. Semi-crystalline structure–dielectric property relationship and electrical conduction in a biaxially oriented poly(vinylidene fluoride) film under high electric fields and high temperatures. ACS Appl Mater Interfaces 2015;7:19894–905.
[6] Zhang QM, Bharti V, Zhao X. Giant electrostriction and relaxor ferroelectric behavior in electron-irradiated poly(vinylidene fluoride-trifluoroethylene) copolymer. Science 1998:2101–4.
[7] Chu B, Zhou X, Ren K, Neese B, Lin M, Wang Q, et al. A dielectric polymer with high electric energy density and fast discharge speed. Science 2006;313:334–6.
[8] Li W, Jiang L, Zhang X, Shen Y, Nan CW. High-energy-density dielectric films based on polyvinylidene fluoride and aromatic polythiourea for capacitors. J Mater Chem A 2014;2:15803–7.
[9] Jiang L, Li W, Zhu J, Huo X, Luo L, Zhu Y. Great reduction of loss at high electric field in the polyvinylidene fluoride/aromatic polythiourea blend films along with an irreversible phase transition. Appl Phys Lett 2015;106:052901.
[10] Zhang S, Zou C, Kushner DI, Zhou X, Orchard RJ, Zhang N, et al. Semicrystalline polymers with high dielectric constant, melting temperature, and charge–discharge efficiency. IEEE Trans Dielectr Electr Insul 2012;19:1158–66.
[11] Gadinski MR, Han K, Li Q, Zhang G, Reainthippayasakul W, Wang Q. High energy density and breakdown strength from β and γ phases in poly (vinylidene fluoride-co-bromotrifluoroethylene) copolymers. ACS Appl Mater Interfaces 2014;6:18981–8.
[12] Carr JM, Mackey M, Flandin L, Schuele D, Zhu L, Baer E. Effect of biaxial orientation on dielectric and breakdown properties of poly(ethylene terephthalate)/poly(vinylidene fluoride-cotetrafluoroethylene) multilayer films. J Polym Sci B: Polym Phys 2013;51:882–96.
[13] Zhou Z, Carr J, Mackey M, Yin K, Schuele D, Zhu L, et al. Interphase/interface modification on the dielectric properties of polycarbonate/poly (vinylidene fluoride-co-hexafluoropropylene) multilayer films for high-energy density capacitors. J Polym Sci B: Polym Phys 2013;51:978–91.
[14] Wolak MA, Pan M-J, Wan A, Shirk JS, Mackey M, Hiltner A, et al. Dielectric response of structured multilayered polymer films fabricated by forced assembly. Appl Phys Lett 2008;92:113301.
[15] Tseng JK, Tang S, Zhou Z, Mackey M, Carr JM, Mu R, et al. Interfacial polarization and layer thickness effect on electrical insulation in multilayered polysulfone/poly(vinylidene fluoride) films. Polymer 2014;55:8–14.
[16] Mackey M, Schuele DE, Zhu L, Flandin L, Wolak MA, Shirk JS, et al. Reduction of dielectric hysteresis in multilayered films via nanoconfinement. Macromolecules 2012;45:1954–62.
[17] Shen Y, Lin Y, Zhang QM. Polymer nanocomposites with high energy storage densities. MRS Bull 2015;40:433–58.
[18] An L, Boggs SA, Calame JP. Energy storage in polymer films with high dielectric constant fillers. In: Proceedings of the 2008 IEEE international power modulators and high voltage conference, Las Vegas, NV. p. 552–5.
[19] An AL, Boggs SA. What is "nano" in the context of a filled dielectric? In: Conference record of the 2006 IEEE international symposium on electrical insulation, 2006, Toronto, Ont.. p. 273–6.
[20] Dang ZM, Yuan JK, Zha JW, Zhou T, Li ST, Hu GH. Fundamentals, processes and applications of high-permittivity polymer–matrix composites. Prog Mater Sci 2012;57:660–723.
[21] Dang ZM, Yuan JK, Yao SH, Liao RJ. Flexible nanodielectric materials with high permittivity for power energy storage. Adv Mater 2013;25:6334–65.
[22] Huang X, Jiang P. Core–shell structured high-k polymer nanocomposites for energy storage and dielectric applications. Adv Mater 2015;27:546–54.
[23] Dang ZM, Lin YH, Nan CW. Novel ferroelectric polymer composites with high dielectric constants. Adv Mater 2003;19:1625–9.
[24] Rao Y, Wong CP. Ultra high dielectric constant polymer metal composite for embedded capacitor application. US patent 6864306; 2005.
[25] Dang ZM, Wang HY, Zhang YH, Qi JQ. Morphology and dielectric property of homogenous $BaTiO_3$/PVDF nanocomposites prepared via the natural adsorption action of nanosized $BaTiO_3$. Macromol Rapid Commun 2005;26:1185–9.
[26] Sharma V, Wang CC, Lorenzini RG, Ma R, Zhu Q, Sinkovits DW, et al. Rational design of all organic polymer dielectrics. Nat Commun 2014;5:4845.
[27] Wang CC, Pilania G, Boggs S, Kumar S, Breneman C, Ramprasad R. Computational strategies for polymer dielectrics design. Polymer 2014;55:979–88.
[28] Mannodi-Kanakkithodi A, Treich G, Huan TD, Ma R, Cao Y, Sotzing G, et al. Rational co-design of polymer dielectrics for energy storage. Adv Mater 2016. http://dx.doi.org/10.1002/adma.201600377 [in press].
[29] Hohenberg P, Kohn W. Inhomogeneous electron gas. Phys Rev 1964;136:B864–71.
[30] Kohn W, Sham LJ. Self-consistent equations including exchange and correlation effects. Phys Rev 1965;140:A1133–8.
[31] Baroni S, de Gironcoli S, Dal Corso A, Giannozzi P. Phonons and related crystal properties from density–functional perturbation theory. Rev Mod Phys 2001;73:515–62.
[32] Baldwin AF, Huan TD, Ma R, Mannodi-Kanakkithodi A, Tefferi M, Katz N, et al. Rational design of organotin polyesters. Macromolecules 2015;48:2422–8.
[33] Baldwin AF, Ma R, Mannodi-Kanakkithodi A, Huan TD, Wang CC, Tefferi M, et al. Poly(dimethyltin glutarate) as a prospective material for high dielectric applications. Adv Mater 2015;27:346–51.
[34] Ma R, Baldwin AF, Wang CC, Offenbach I, Cakmak M, Ramprasad R, et al. Rationally designed polyimides for high-energy density capacitor applications. ACS Appl Mater Interfaces 2014;6:10445–51.
[35] Lorenzini RG, Kline WM, Wang CC, Ramprasad R, Sotzing GA. The rational design of polyurea & polyurethane dielectric materials. Polymer 2013;54:3529–33.
[36] Ma R, Sharma V, Baldwin AF, Tefferi M, Offenbach I, Cakmak M, et al. Rational design and synthesis of polythioureas as capacitor dielectrics. J Mater Chem A 2015;3:14845–52.
[37] Sun Y, Boggs AS, Ramprasad S. The intrinsic electrical breakdown strength of insulators from first principles. Appl Phys Lett 2012;101:132906.
[38] Sun Y, Bealing C, Boggs SA, Ramprasad R. 50+ years of intrinsic breakdown. IEEE Electr Insul Mag 2013;29:8–15.
[39] Sun Y, Boggs S, Ramprasad R. The effect of dipole-induced scattering on the intrinsic breakdown field of polymers. IEEE Trans Dielectr Electr Insul 2015;22:495–502.
[40] Huzayyin A, Boggs S, Ramprasad R. Quantum mechanical studies of carbonyl impurities in dielectric polyethylene. IEEE Trans Dielectr Electr Insul 2010;17:920–5.
[41] Huzayyin A, Boggs S, Ramprasad R. Density functional analysis of chemical impurities in dielectric polyethylene. IEEE Trans Dielectr Electr Insul 2010;17:926–30.
[42] Chen L, Huan TD, Wang CC, Ramprasad R. Unraveling the luminescence signatures of chemical defects in polyethylene. J Chem Phys 2015;143:124907.
[43] Chen L, Huan TD, Quintero Y, Ramprasad R. Charge injection barriers at metal/polyethylene interfaces. J Mater Sci 2016;51:506–12.
[44] Jorgensen WL, Ulmschneider JP, Tirado-Rives J. Free energies of hydration from a generalized born model and an all-atom force field. J Phys Chem B 2004;108:16264–70.
[45] Wang J, Wolf RM, Caldwell JW, Kollman PA, Case DA. Development and testing of a general amber force field. J Comput Chem 2004;25:1157–74.
[46] Vanommeslaeghe K, MacKerell Jr AD. Automation of the CHARMM General Force Field (CGenFF) I: bond perception and atom typing. J Chem Inf Model 2012;52:3144–54.
[47] Vanommeslaeghe K, Prabhu Raman E, MacKerell Jr AD. Automation of the CHARMM General Force Field (CGenFF) II: assignment of bonded parameters and partial atomic charges. J Chem Inf Model 2012;52:3155–68.

[48] Rigby D, Roe R-J. Molecular dynamics simulation of polymer liquid and glass. I. Glass transition. J Chem Phys 1987;87:7285–92.
[49] Bitsanis I, Hadziioannou G. Molecular dynamics simulations of the structure and dynamics of confined polymer melts. J Chem Phys 1990;92:3827–47.
[50] Bennemann C, Paul W, Binder K, Dünweg B. Molecular-dynamics simulations of the thermal glass transition in polymer melts: α-relaxation behavior. Phys Rev E 1998;57:843–51.
[51] Moreno M, Casalegno M, Raos G, Meille SV, Po R. Molecular modeling of crystalline alkylthiophene oligomers and polymers. J Phys Chem B 2010;114:1591–602.
[52] Hautier G, Jain A, Ong SP. From the computer to the laboratory: materials discovery and design using first-principles calculations. J Mater Sci 2012;47:7317–40.
[53] Mueller T, Kusne AG, Ramprasad R. In: Parrill AL, Lipkowitz KB, editors. Reviews in computational chemistry. New York, USA: Wiley; 2016.
[54] Pilania G, Wang CC, Jiang X, Rajasekaran S, Ramprasad R. Accelerating materials property predictions using machine learning. Sci Rep 2013;3:2810.
[55] Huan TD, Mannodi-Kanakkithodi A, Ramprasad R. Accelerated materials property predictions and design using motif-based fingerprints. Phys Rev B 2015;92:014106.
[56] Mannodi-Kanakkithodi A, Pilania G, Huan TD, Lookman T, Ramprasad R. Machine learning strategy for accelerated design of polymer dielectrics. Sci Rep 2016;6:20952.
[57] Baldwin AF, Ma R, Huan TD, Cao Y, Ramprasad R, Sotzing GA. Effect of incorporating aromatic and chiral groups on the dielectric properties of poly (dimethyltin esters). Macromol Rapid Commun 2014;35:2082–8.
[58] Kresse G, Furthmüller J. Efficiency of ab-initio total energy calculations for metals and semiconductors using a plane-wave basis set. Comput Mater Sci 1996;6:15–50.
[59] Kresse G, Furthmüller J. Efficient iterative schemes for ab initio total-energy calculations using a plane-wave basis set. Phys Rev B 1996;54:11169–86.
[60] Christensen RM. Theory of viscoelasticity: an introduction. New York, USA: Academic Press; 1971.
[61] Han J, Boyd RH. Molecular packing and small-penetrant diffusion in polystyrene: a molecular dynamics simulation study. Polymer 1996;37:1797–804.
[62] Müller-Plathe F. Local structure and dynamics in solvent-swollen polymers. Macromolecules 1996;29:4782–91.
[63] Ho J, Jow TR. High field conduction in biaxially oriented polypropylene at elevated temperature. IEEE Trans Dielectr Electr Insul 2012;19:990–5.
[64] Arnold D, Cartier E, DiMaria DJ. Theory of high-field electron transport and impact ionization in silicon dioxide. Phys Rev B 1994;49:10278–97.
[65] von Hippel A. Electric breakdown of solid and liquid insulators. J Appl Phys 1937;8:815–32.
[66] Zener CM. A theory of the electrical breakdown of solid dielectrics. Proc R Soc 1934;145:523–9.
[67] Fröhlich H. Theory of electrical breakdown in ionic crystals. Proc R Soc Lond, Ser A 1937;160:230–41.
[68] Fröhlich H. Theory of dielectric breakdown. Nature 1943;151:339–40.
[69] Fröhlich H. On the theory of dielectric breakdown in solids. Proc R Soc Lond, Ser A 1947;188:521–32.
[70] Sparks M, Mills DL, Warren R, Holstein T, Maradudin AA, Sham LJ, et al. Theory of electron-avalanche breakdown in solids. Phys Rev B 1981;24:3519–36.
[71] Cartier E, Pfluger P. Transport and relaxation of hot conduction electrons in an organic dielectric. Phys Rev B 1986;34:8822–7.
[72] Sjakste J, Vast N, Tyuterev V. Ab initio method for calculating electron–phonon scattering times in semiconductors: application to GaAs and GaP. Phys Rev Lett 2007;99:236405.
[73] Restrepo OD, Varga K, Pantelides ST. First-principles calculations of electron mobilities in silicon: phonon and Coulomb scattering. Appl Phys Lett 2009;94:212103.
[74] Borysenko KM, Mullen JT, Barry EA, Paul S, Semenov YG, Zavada JM, et al. First-principles analysis of electron–phonon interactions in graphene. Phys Rev B 2010;81:121412(R).
[75] Jacoboni C, Reggiani L. The Monte Carlo method for the solution of charge transport in semiconductors with applications to covalent materials. Rev Mod Phys 1983;55:645–705.
[76] Fischetti MV, Laux SE. Monte Carlo analysis of electron transport in small semiconductor devices including band-structure and space-charge effects. Phys Rev B 1988;38:9721–45.
[77] Fischetti MV, Laux SE. Monte Carlo simulation of transport in technologically significant semiconductors of the diamond and zinc-blende structures – part II: submicrometer MOSFET's. IEEE Trans Electron Devices 1991;38:650–60.
[78] Smirnov BM. Physics of ionized gas. New York, USA: Wiley & Sons; 2001.
[79] Sharbaugh AH, Devins JC, Rzad SJ. Review of past work on liquid breakdown. IEEE Trans Electr Insul 1980;EI-15:167–70.
[80] Balygin IE. Electrical breakdown of liquid dielectrics (a review). Foreign Technology Division, Wright-Patterson Air Force Base, AD-752 819; 1972.
[81] Cao Y, Boggs S. Mechanisms of high field electroluminescence and determination of the space charge limited field in polymeric dielectrics. IEEE Trans Dielectr Electr Insul 2005;12:690–9.
[82] Boggs SA. Very high field phenomena in dielectrics. IEEE Trans Dielectr Electr Insul 2005;12:929–38.
[83] Qiao B, Teyssedre G, Laurent C. Uncover the electroluminescence in wide band gap polymers. J Phys D: Appl Phys 2015;48:405102.
[84] Xu CC, Ho J, Boggs SA. Automatic breakdown voltage measurement of polymer films. IEEE Electr Insul Mag 2008;24:30–4.
[85] McPherson J, Kim J, Shanware A, Mogul H, Rodriguez J. Proposed universal relationship between dielectric breakdown and dielectric constant. Tech Dig – Int Electron Devices Meet 2002;2002:633–6.
[86] Wilson KJ, Less EG. Intrinsic photoconduction and photoemission in polyethylene. J Phys C: Solid State Phys 1973;6:3110–20.
[87] George RA, Martin DH, Wilson EG. The ultraviolet spectra of polyethylene and long-chain paraffins. J Phys C: Solid State Phys 1972;5:871–8.
[88] Salaneck WR. Photoelectron spectroscopy of polyconjugated polymer surfaces and interfaces. Rep Prog Phys 1991;54:1215–49.
[89] Tanaka T. Optical absorption and electrical conduction in polyethylene. J Appl Phys 1973;44:2430–2.
[90] Perdew JP. Density functional theory and the band gap problem. Int J Quant Chem 1985;28:497–523.
[91] Ramprasad R, Glassford KM, Adams JB, Masel RI. CO on Pd(110): determination of the optimal adsorption site. Surf Sci 1996;360:31–42.
[92] Heyd J, Scuseria GE, Ernzerhof M. Hybrid functionals based on a screened Coulomb potential. J Chem Phys 2003;118:8207–25.
[93] Hedin L. New method for calculating the one-particle Green's function with application to the electron–gas problem. Phys Rev 1965;139:A796–823.
[94] van Schilfgaarde M, Kotani Takao, Faleev S. Quasiparticle self-consistent GW theory. Phys Rev Lett 2006;96:226402.
[95] Hybertsen MS, Louie SG. First-principles theory of quasiparticles: calculation of band gaps in semiconductors and insulators. Phys Rev Lett 1985;55:1418–21.
[96] Dissado LA, Mazzanti G, Montanari GC. The role of trapped space charges in the electrical aging of insulating materials. IEEE Trans Dielectr Electr Insul 1997;4:496–506.
[97] Mazzanti G, Montanari GC. Electrical aging and life models: the role of space charge. IEEE Trans Dielectr Electr Insul 2005;12:876–90.
[98] Massines F, Tiemblo P, Teyssedre G, Laurent C. On the nature of the luminescence emitted by a polypropylene film after interaction with a cold plasma at low temperature. J Appl Phys 1997;81:937–43.
[99] Ito T, Kaneko D, Ohki Y. Origins of photoluminescence bands induced by ultraviolet photons in polyethylene. In: 2002 Annual report conference on electrical insulation and dielectric phenomena. p. 856–9.
[100] Teyssedre G, Cissé L, Laurent C, Massines L, Tiemblo P. Spectral analysis of optical emission due to isothermal charge recombination in polyolefins. IEEE Trans Dielectr Electr Insul 1998;5:527–35.
[101] Teyssedre G, Laurent C. Semi-quantitative analysis of photoluminescence in thermoelectrically aged cables: I – identification of optical signatures. IEEE Trans Dielectr Electr Insul 2009;16:1180–8.
[102] Zlatkevich L. Luminescence techniques in solid state polymer research. New York: Marcel Dekker Inc.; 1989.
[103] Debye P, Edwards JO. Long lifetime phosphorescence and the diffusion process. J Chem Phys 1952;20:236–9.

[104] Hama Y, Kimura Y, Tsumura M, Omi N. Studies of the recombination of cation–electron pairs by long-range tunnelling, as studied by ITL measurements in irradiated polymers. J Chem Phys 1980;53:115–22.
[105] Hagekyriakou J, Fleming RJ. Determination of the kinetic order of thermoluminescence in the presence of a distribution of electron trap activation energies. J Phys D: Appl Phys 1982;15:163–76.
[106] Teyssedre G, Laurent C, Montanari GC, Perego G. Charge recombination induced luminescence of chemically modified cross-linked polyethylene materials. IEEE Trans Dielectr Electr Insul 2009;16:232–40.
[107] Teyssedre G, Reinecke H, Corrales T, Navarro R, Garcia N, Tiemblo P. Study of secondary relaxations in poly(vinyl chloride) by phosphorescence decay. Effect of the chemical structure and the concentration of luminescent probes. J Photochem Photobiol A: Chem 2007;187:222–32.
[108] Kivits P, Hagebeuk HJL. Evaluation of the model for thermally stimulated luminescence and conductivity; reliability of trap depth determinations. J Lumin 1977;15:1–27.
[109] Teyssedre G, Tardieu G, Laurent C. Characterization of crosslinked polyethylene materials by luminescence techniques. J Mater Sci 2002;37:1599–609.
[110] Freysoldt C, Grabowski B, Hickel T, Neugebauer J, Kresse G, Janotti A, et al. First-principles calculations for point defects in solids. Rev Mod Phys 2014;86:253–305.
[111] Ramprasad R, Zhu H, Rinke P, Scheffler M. New perspective on formation energies and energy levels of point defects in nonmetals. Phys Rev Lett 2012;108:066404.
[112] Yan Q, Janotti A, Scheffler M, Van de Walle CG. Origins of optical absorption and emission lines in AlN. Appl Phys Lett 2014;105:111104.
[113] Bealing C, Ramprasad R. An atomistic description of the high-field degradation of dielectric polyethylene. J Chem Phys 2014;139:174904.
[114] Meunier M, Quirke N, Aslanides A. Molecular modeling of electron traps in polymer insulators: chemical defects and impurities. J Chem Phys 2001;115:2876–81.
[115] Anta JA, Marcelli G, Meunier M, Quirke N. Models of electron trapping and transport in polyethylene: current–voltage characteristics. J Appl Phys 2002;92:1002–8.
[116] Gruning M, Marini A, Rubio A. Density functionals from many-body perturbation theory: the band gap for semiconductors and insulators. J Chem Phys 2006;124:154108.
[117] Yan Q, Janotti A, Scheffler M, Van de Walle CG. Role of nitrogen vacancies in the luminescence of Mg-doped GaN. Appl Phys Lett 2012;100:142110.
[118] Lewis TJ. Ageing – a perspective. IEEE Electr Insul Mag 2001;17:6–16.
[119] Tzimas A, Rowland SM, Dissado LA. Effect of electrical and thermal stressing on charge traps in XLPE cable insulation. IEEE Trans Dielectr Electr Insul 2012;19:2145–54.
[120] Mazzanti G, Montanari GC, Alison JM. A space charge based method for the estimation of apparent mobility and trap depth as markers for insulation degradation-theoretical basis and experimental validation. IEEE Trans Dielectr Electr Insul 2003;10:187–97.
[121] Simmons JG, Tam MC. Theory of isothermal currents and the direct determination of trap parameters in semiconductors and insulators containing arbitrary trap distributions. Phys Rev B 1972;7:3706–13.
[122] Mizutani T, Suzuoki Y, Hanai M, Ieda M. Determination of trapping parameters from TSC in polyethylene. Jpn J Appl Phys 1982;21:1639–41.
[123] Ieda M. Carrier injection, space charge and electrical breakdown in insulating polymers. IEEE Trans Electr Insul 1987;22:261–7.
[124] Zhu Z, Zhang Y, An Z, Zheng F. A novel method for distribution of trap levels in dielectric by photo-stimulated discharge. In: 2010 International conference on solid dielectrics, Potsdam. p. 1–4.
[125] Cartier E, Pfluger P. Detection of hot electron-induced radiation damage in organic dielectrics by exoelectron emission from thin films. IEEE Trans Electr Insul 1987;22:123–8.
[126] Boggs S, Kuang J. High field effects in solid dielectrics. IEEE Electr Insul Mag 1998;14:5–12.
[127] Shimizu N, Laurent C. Electrical tree initiation. IEEE Trans Dielectr Electr Insul 1998;5:651–9.
[128] Fothergill JC, Montanari GC, Stevens GC, Laurent C, Teyssedre, Dissado LA, et al. Electrical, microstructural, physical and chemical characterization of HV XLPE cable peelings for an electrical aging diagnostic data base. IEEE Trans Dielectr Electr Insul 2003;10:514–27.
[129] Laurent C, Teyssedre G, Le Roy S, Baudoin F. Charge dynamics and its energetic features in polymeric materials. IEEE Trans Dielectr Electr Insul 2013;20:357–81.
[130] Le Roy S, Teyssedre G, Laurent C. Charge transport and dissipative processes in insulating polymers: joining experiments and model. IEEE Trans Dielectr Electr Insul 2005;12:644–54.
[131] Baudoin F, Mills DH, Lewin PL, Le Roy S, Teyssedre G, Laurent C. Modeling electroluminescence in insulating polymers under ac stress: effect of excitation waveform. J Phys D: Appl Phys 2011;44:165402.
[132] Laurent C, Massines F, Mayoux C, Ryder D, Olliff C. Comparison between photo- and electro-induced luminescence spectra of polyethylene. In: IEEE conference on electrical insulation and dielectric phenomena, Virginia Beach, USA. p. 93–6.
[133] Jones JP, Llewellyn JP, Lewis TJ. The contribution of field-induced morphological change to the electrical aging and breakdown of polyethylene. IEEE Trans Dielectr Electr Insul 2005;12:951–66.
[134] Xu CC, Boggs S. Measurement of resistive and absorption currents in capacitor films up to breakdown. In: 2006 IEEE international symposium on electrical insulation, Toronto, Ont.. p. 249–52.
[135] Xu CC, Boggs S. Simulation of high field resistive and absorption currents in semicrystalline polymer films. In: 2006 IEEE international symposium on electrical insulation, Toronto, Ont.. p. 358–61.
[136] Peacock A. Handbook of polyethylene: structures: properties, and applications. 1st ed. New York, US: CRC Press; 2000.
[137] Qin S, Ho J, Rabuffi M, Borelli G, Jow TR. Implications of the anisotropic thermal conductivity of capacitor windings. IEEE Electr Insul Mag 2011;27:7–13.
[138] Koike Y, Cakmak M. The influence of molten fraction on the uniaxial deformation behavior of polypropylene: real time mechano-optical and atomic force microscopy observations. J Polym Sci: Polym Phys 2006;44:925–41.
[139] Koike Y, Cakmak M. Role of molten fraction on the structural evolution in stretching and cooling of crosslinked low-density polyethylene: real-time mechano-optical measurements. J Polym Sci B: Polym Phys 2005;43:1825–41.
[140] Koike Y, Cakmak M. Real time development of structure in partially molten state stretching of polypropylene as detected by spectral birefringence technique: effect of isotacticity. J Macromol Sci B: Phys 2006;45:13–37.
[141] Oganov AR. Modern methods of crystal structure prediction. Weinheim, Germany; 2011.
[142] Atahan-Evrenk Ş, Aspuru-Guzik A. Prediction and calculation of crystal structures: methods and applications. Springer International Publishing; 2014.
[143] Maddox J. Crystals from first principles. Nature 1988;335:201.
[144] Zhu Q, Sharma V, Oganov AR, Ramprasad R. Predicting polymeric crystal structures by evolutionary algorithms. J Chem Phys 2014;141:154102.
[145] Huan TD, Sharma V, Rossetti Jr GA, Ramprasad R. Pathways towards ferroelectricity in hafnia. Phys Rev B 2014;90:064111.
[146] Sharma H, Sharma V, Huan TD. Exploring $PtSO_4$ and $PdSO_4$ phases: an evolutionary algorithm based investigation. Phys Chem Chem Phys 2015;17:18146–51.
[147] Oganov AR, Glass CW. Crystal structure prediction using ab initio evolutionary techniques: principles and applications. J Chem Phys 2006;124:244704.
[148] Goedecker S. Minima hopping: an efficient search method for the global minimum of the potential energy surface of complex molecular systems. J Chem Phys 2004;120:9911–7.
[149] Amsler M, Goedecker S. Crystal structure prediction using the minima hopping method. J Chem Phys 2010;133:224104.
[150] Wang Y, Lv J, Zhu L, Ma Y. CALYPSO: a method for crystal structure prediction. Comput Phys Commun 2012;183:2063–70.

[151] Pickard CJ, Needs RJ. Ab initio random structure searching. J Phys: Condens Matter 2011;23:053201.
[152] Chu D, Till M, Zomaya A. Parallel ant colony optimization for 3D protein structure prediction using the HP lattice model. In: 19th IEEE international parallel and distributed processing symposium, Denver, CO. p. 1–7.
[153] Glass CW, Oganov AR, Hansen N. USPEX-evolutionary crystal structure prediction. Comput Phys Commun 2006;175:713–20.
[154] Lovinger AJ, Chua JO, Gryte CC. Studies on the α and β forms of isotactic polypropylene by crystallization in a temperature gradient. J Polym Sci Polym Phys Ed 1977;15:641–56.
[155] Muthukumar M. Modeling polymer crystallization. In: Allegra G, editor. Interphases and mesophases in polymer crystallization III. Berlin, Heidelberg: Springer; 2005. p. 241–74.
[156] Jin J, Chen HY, Muthukumar M, Han CC. Kinetics pathway in the phase separation and crystallization of iPP/OBC blends. Polymer 2013;54:4010–6.
[157] Gee RH, Lacevic N, Fried LE. Atomistic simulations of spinodal phase separation preceding polymer crystallization. Nat Mater 2006;5:39–43.
[158] Gautam S, Balijepalli S, Rutledge GC. Molecular simulations of the interlamellar phase in polymers: effect of chain tilt. Macromolecules 2000;33:9136–45.
[159] Rang HJ, White JL. A double bubble tubular film process to produce biaxially oriented poly(p-phenylene sulfide) (PPS) film. Polym Eng Sci 1990;30:1228–36.
[160] Kanai T, Campbell G. Film processing; 2011.
[161] Schrenk WJ, Chisholm DS, Cleereman KJ, Turner Jr A. Multilayer thermoplastic articles. US patent US 3647612 A 19720307; 1972.
[162] Lee PC, Dooley J. Experimental and numerical analysis of micro/nanolayer coextrusion. J Plast Film Sheeting 2013;29:78–98.
[163] Mackey M, Schuele DE, Zhu L, Baer E. Layer confinement effect on charge migration in polycarbonate/poly(vinylidene fluoride-co-hexafluoropropylene) multilayered films. J Appl Phys 2012;111:113702.
[164] Mackey M, Hiltner A, Baer E, Flandin L, Wolak MA, Shirk JS. Enhanced breakdown strength of multilayered films fabricated by forced assembly microlayer coextrusion. J Phys D: Appl Phys 2009;42:175304.
[165] Hassan MK, Cakmak M. Mechanisms of structural organizational processes as revealed by real time mechano optical behavior of PET film during sequential biaxial stretching. Polymer 2014;55:5245–54.
[166] Hassan M, Cakmak M. Mechano optical behavior of polyethylene terephthalate films during. Polymer 2013;54:6463–70.
[167] Ou X, Cakmak M. Influence of biaxial stretching mode on the crystalline texture in polylactic acid films. Polymer 2008;49:5344–52.
[168] Bicakci S, Cakmak M. Kinetics of rapid structural changes during heat setting of preoriented PEEK/PEI blend films as followed by spectral birefringence technique. Polymer 2002;43:2737–46.
[169] Reed CW, Cichanowski SW. The fundamentals of aging in HV polymer-film capacitors. IEEE Trans Dielectr Electr Insul 1994;1:904–22.
[170] Lewis TJ. Polyethylene under electrical stress. IEEE Trans Dielectr Electr Insul 2002;9:717–29.
[171] Mizutani T, Takai Y, Osawa T, Ieda M. Barrier heights and surface states of metal–polymer (PET) contacts. J Phys D: Appl Phys 1976;9:2253–9.
[172] Taleb M, Teyssèdre G, Le Roy S, Laurent C. Modeling of charge injection and extraction in a metal/polymer interface through an exponential distribution of surface states. IEEE Trans Dielectr Electr Insul 2013;20:311–20.
[173] Chen G, Tanaka Y, Takada T, Zhong L. Effect of polyethylene interface on space charge formation. IEEE Trans Dielectr Electr Insul 2004;11:113–21.
[174] Thielen A, Niezette J, Feyder G, Vanderschueren J. Thermally stimulated current study of space charge formation and contact effects in metal–polyethylene terephthalate film/metal systems. I. Generalities and theoretical model. J Phys Chem Solids 1996;57:1567–80.
[175] Mizutani T, Ikeda S, Ieda M. Oxidation enhanced TSC and TSSP of polyethylene. Jpn J Appl Phys 1986;22:22–6.
[176] Muccigrosso J, Phillips PJ. The morphology of cross-linked polyethylene insulation. IEEE Trans Electr Insul 1978;13:172–8.
[177] Baldo M, Forrest SR. Interface-limited injection in amorphous organic semiconductors. Phys Rev B 2001;64:085201.
[178] Van de Walle CG, Martin RM. Theoretical study of band offsets at semiconductor interfaces. Phys Rev B 1987;35:8154–65.
[179] Shaltaf R, Rignanese G-M, Gonze X, Giustino F, Pasquarello A. Band offsets at the Si/SiO_2 interface from many-body perturbation theory. Phys Rev Lett 2008;100:186401.
[180] Puthenkovilakam R, Chang JP. An accurate determination of barrier heights at the HfO_2/Si interfaces. J Appl Phys 2004;96:2701–7.
[181] Uttamchandani R, Zhang X, Shankar S, Lu G. Chemical tuning of band alignments for Cu/HfO_2 interfaces. Phys Status Solidi B 2015;252:298–304.
[182] Zhu H, Ramprasad R. Effective work function of metals interfaced with dielectrics: a first-principles study of the Pt–HfO_2 interface. Phys Rev B 2011;83:081416.
[183] Zhu H, Ramanath G, Ramprasad R. Interface engineering through atomic dopants in HfO_2-based gate stacks. J Appl Phys 2013;114:114310.
[184] Taleb M, Teyssedre G, Le Roy S. Role of the interface on charge build-up in a low-density polyethylene: surface roughness and nature of the electrode. In: IEEE conference on electrical insulation and dielectric phenomena 2009, Virginia Beach, VA. p. 112–5.
[185] Taylor DM, Lewis TJ. Electrical conduction in polyethylene terephthalate and polyethylene films. J Phys D: Appl Phys 1971;4:1346–57.
[186] Qi X, Boggs SA. Electrothermal failure of metallized film capacitor end connections – computation of temperature rise at connection spots. J Appl Phys 2003;94:4449–56.
[187] Hill GJ, Straight JH. Selection of dielectric materials for use in energy-storage capacitors. In: Symposium on high-energy-density capacitors and dielectric materials, Washington, DC. p. 105–11.
[188] MacDougall F, Ennis J, Yang XH, Seal K, Phatak S, Spinks B, et al. Large high energy density pulse discharge capacitor characterization. In: The 15th IEEE international pulsed power conference, Monterey, CA. p. 1215–8.
[189] Dang ZM, Yao SH, Xu HP. Effect of tensile strain on morphology and dielectric property in nanotubes/polymer composites. Appl Phys Lett 2007;90:012907.
[190] Dang ZM, Wang L, Yin Y, Zhang Q, Lei QQ. Giant dielectric permittivities in functionalized carbon–nanotube/electroactivepolymer. Adv Mater 2007;19:852–7.
[191] Wang L, Dang ZM. Carbon nanotube composites with high dielectric constant at low percolation threshold. Appl Phys Lett 2005;87:042903.
[192] Zhang QM, Li HF, Poh M, Xia F, Cheng Z-Y, Xu H, et al. An all-organic composite actuator material with a high dielectric constant. Nature 2002;419:284–7.
[193] Yuan X, Matsuyama Y, Chung TCM. Synthesis of functionalized isotactic polypropylene dielectrics for electric energy storage applications. Macromolecules 2010;43:4011–5.
[194] Zhang G, Li H, Antensteiner M, Chung TCM. Synthesis of functional polypropylene containing hindered phenol stabilizers and applications in metallized polymer film capacitors. Macromolecules 2015;48:2925–34.
[195] Zhang M, Yuan X, Wang L, Chung TCM, Huang T, deGroot W. Synthesis and characterization of well-controlled isotactic polypropylene ionomers containing ammonium ion groups. Macromolecules 2014;47:571–81.
[196] Gupta S, Yuan X, Chung TCM, Kumar S, Cakmak M, Weiss RA. Effect of hydroxyl-functionalization on the structure and properties of polypropylene. Macromolecules 2013;46:5455–63.
[197] Wang CC, Pilania G, Ramprasad R, Agarwal M, Misra M, Kumar S, et al. Dielectric permittivity enhancement in hydroxyl functionalized polyolefins via cooperative interactions with water. Appl Phys Lett 2013;102:152901.
[198] Misra M, Agarwal M, Sinkovits DW, Kumar SK, Wang CC, Pilania G, et al. Enhanced polymeric dielectrics through incorporation of hydroxyl groups. Macromolecules 2014;47:1122–9.
[199] Wu S, Li W, Lin M, Burlingame Q, Chen Q, Payzant A, et al. Aromatic polythiourea dielectrics with ultrahigh breakdown field strength, low dielectric loss, and high electric energy density. Adv Mater 2013;25:1734–8.
[200] Pilania G, Wang CC, Wu K, Sukumar N, Breneman C, Sotzing G, et al. New group IV chemical motifs for improved dielectric permittivity of polyethylene. J Chem Inf Model 2013;53:879–86.
[201] Wang CC, Ramprasad R. Novel hybrid polymer dielectrics based on group 14 chemical motifs. Int J High Speed Electron Syst 2014;23:1420002.

[202] Mannodi-Kanakkithodi A, Wang CC, Ramprasad R. Compounds based on group 14 elements: building blocks for advanced insulator dielectrics design. J Mater Sci 2015;50:801–7.
[203] Huan TD, Mannodi-Kanakkithodi A, Kim C, Sharma V, Pilania G, Ramprasad R. A polymer dataset for accelerated property prediction and design. Sci Data 2016;3:160012.
[204] Materials Genome Initiative (MGI). <https://www.whitehouse.gov/mgi>.
[205] de Pablo JJ, Jones B, Kovacs CL, Ozoliņš V, Ramirez AP. The materials genome initiative, the interplay of experiment, theory and computation. Curr Opin Solid State Mater Sci 2014;18:99–117.